NASA TN D-388

TECHNICAL NOTE

D-388

TRANSONIC PERFORMANCE CHARACTERISTICS

OF SEVERAL JET NOISE SUPPRESSORS

By James W. Schmeer, Leland B. Salters, Jr.,
and Marlowe D. Cassetti

Langley Research Center
Langley Field, Va.

NATIONAL AERONAUTICS AND SPACE ADMINISTRATION

WASHINGTON July 1960

NATIONAL AERONAUTICS AND SPACE ADMINISTRATION

TECHNICAL NOTE D-388

TRANSONIC PERFORMANCE CHARACTERISTICS OF SEVERAL JET NOISE SUPPRESSORS

By James W. Schmeer, Leland B. Salters, Jr., and Marlowe D. Cassetti

SUMMARY

An investigation of the transonic performance characteristics of several noise-suppressor configurations has been conducted in the Langley 16-foot transonic tunnel. The models were tested statically and over a Mach number range from 0.70 to 1.05 at an angle of attack of 0°. The primary jet total-pressure ratio was varied from 1.0 (jet off) to about 4.5. The effect of secondary air flow on the performance of two of the configurations was investigated. A hydrogen peroxide turbojet-engine simulator was used to supply the hot-jet exhaust.

An 8-lobe afterbody with centerbody, short shroud, and secondary air had the highest thrust-minus-drag coefficients of the six noise-suppressor configurations tested. The 12-tube and 12-lobe afterbodies had the lowest internal losses. The presence of an ejector shroud partially shields the external pressure distribution of the 8-lobe afterbody from the influence of the primary jet. A ring-airfoil shroud increased the static thrust of the annular nozzle but generally decreased the thrust minus drag at transonic Mach numbers.

INTRODUCTION

Many investigations have been made of the noise-reducing effectiveness and internal aerodynamic losses of various jet-noise suppressors. The overall performance characteristics at cruising speed, however, have not been thoroughly investigated. Some performance data on full-scale noise suppressors at flight Mach numbers up to 0.5 are given in reference 1 and cold-air tests with one-fifth-scale model suppressors at Mach numbers of 0.65 to 1.10 are reported in reference 2. The purpose of the present investigation was to evaluate the relative performance penalties of several typical noise suppressors with hot-jet exhaust at high subsonic and transonic flight speeds.

The investigation was conducted in the Langley 16-foot transonic tunnel at Mach numbers from 0.70 to either 0.95 or 1.05 depending on nozzle configuration. The tests were made at an angle of attack of 0° and jet total-pressure ratios from 1.0 (jet off) to about 4.5. The propulsive thrust was measured (gross thrust minus afterbody drag) for each noise-suppressor nozzle and compared with a standard nozzle. The internal losses were evaluated from static tests. No noise measurements were made in this investigation but noise-suppression qualities for similar type nozzles are available. (See refs. 1 and 3 for instance.)

SYMBOLS

A	area, sq ft
$C_{D,a}$	afterbody pressure-drag coefficient, $C_{D,\beta} + C_{D,b}$
$C_{D,b}$	base drag coefficient, $-C_{p,b} \frac{A_b}{A_{max}}$
$C_{D,\beta}$	boattail drag coefficient (includes centerbody where used), $-\sum \frac{C_p A_l}{A_{max}}$
C_{F-D}	thrust-minus-drag coefficient, $\frac{\text{Thrust minus drag}}{qA_e}$
$C_{F,o}$	static thrust coefficient, $\frac{F}{p_o A_e}$
$C_{F,i}$	ideal static thrust coefficient, $\frac{F_i}{p_o A_e}$
C_p	pressure coefficient, $\frac{p_l - p_\infty}{q}$
D	drag, lb
d	diameter, in.
F	measured jet thrust, lb

F_i ideal thrust for complete isentropic expansion of primary flow, $\frac{w}{g}\sqrt{2Rg\,\frac{\gamma}{\gamma-1}\,T_{t,j}\left[1-\left(\frac{p_\infty}{p_{t,j}}\right)^{\frac{\gamma-1}{\gamma}}\right]}$

g gravitational acceleration, ft/sec^2

L distance from primary jet exit to shroud exit, in.

l length of standard afterbody, 11.84 in.

M free-stream Mach number

m mass flow, slugs/sec

p static pressure, lb/sq ft

p_t total pressure, lb/sq ft

$p_{t,j}/p_\infty$ ratio of primary jet total pressure to free-stream static pressure

q free-stream dynamic pressure, lb/sq ft

R gas constant, $ft/^oR$

r radius, in.

T_t stagnation temperature, ^oR

w measured weight flow, lb/sec

x longitudinal distance from reference point, positive rearward, in.

γ ratio of specific heats

ϕ meridian angle, positive counterclockwise looking forward from afterbody exit, deg

Subscripts:

a afterbody

b base

e	primary jet exit
i	ideal
j	jet
l	local
max	maximum
o	barometric
p	primary
s	secondary
sl	seal
std	standard nozzle
t	total
∞	free stream (ambient static)
bal	balance

APPARATUS

Wind Tunnel

This investigation was conducted in the Langley 16-foot transonic tunnel which is a single-return atmospheric wind tunnel with an octagonal slotted test section. It has a speed range from a Mach number of 0.20 to about 1.10 and the Mach number is varied over this range by variation of tunnel drive power.

Model and Support System

A photograph of the 8-lobe noise suppressor mounted on the pylon-nacelle model in the Langley 16-foot transonic tunnel is shown in figure 1. A sketch of the pylon-nacelle model with standard nozzle is shown in figure 2. The nacelle was supported in the tunnel by means of a sweptforward pylon which was fixed to a conventional sting. The nacelle forebody was fixed rigidly to the pylon and the turbojet simulator with afterbody were attached to the nacelle through a strain-gage

thrust balance. The annular gap which provided clearance between the nacelle forebody and afterbody was covered by a thin annular ring to shield the external flow from the effects of the gap (which varied in size with temperature change) and yet prevent contact between the surfaces. (See detail A, fig. 2.) The jet simulator unit produced a hot jet exhaust at a temperature of about 1,350° F and is described in reference 4.

Afterbody Configurations

Standard nozzle.- The standard nozzle, shown in figure 3, was a simple convergent nozzle with no noise-suppressor characteristics and was designed solely as a basis of comparison with the noise-suppressor nozzles. The shape of the afterbody was chosen to represent a typical turbojet nacelle installation. The rearmost part consisted of a simple conical section with a boattail angle of 16°.

Noise-suppressor nozzles.- Six noise-suppressor nozzle configurations were tested: a 12-lobe nozzle (fig. 4(a)), a 12-tube nozzle (fig. 4(b)), an annular nozzle, an annular nozzle with shroud (fig. 4(c)), an 8-lobe nozzle with long shroud, and an 8-lobe nozzle with short shroud (fig. 4(d)).

The 8-lobe nozzles had provision for secondary air flow between the nozzle and the shroud, the secondary air exit being concentric with the primary jet exit. The secondary air was supplied by a compressed air line routed through the sting. It contained a flexible link, in the form of plastic tubing, to minimize restraint. With the exception of the annular nozzle those parts of the noise-suppressor afterbodies forward of the noise-reducing elements (such as the lobes in the case of the 12-lobe configuration) were shaped similar to that of the standard afterbody in order that the performance differences would represent those penalties attributable to noise-suppression qualities. In the case of the 12-tube and 12-lobe nozzles, there were some area differences in the transition section from $x/l = 0.50$ back to the beginning of the actual nozzle sections. The afterbody ordinates for each configuration are included in figure 4.

Instrumentation

Thrust minus drag was measured by means of a one-component strain-gage balance shown in figure 2. Static-pressure orifices were located on the external surfaces and base of the standard and 8-lobe nozzles at places indicated in figures 3 and 4(d). Total pressure and temperature were measured for all primary jets and for the secondary air of the 8-lobe nozzle.

Pressures were transmitted to fast response electrical pressure transducers by means of tubing routed through the support system. The electrical signals of the pressure transducers, thermocouples, and strain-gage balance were transmitted to recording oscillographs.

METHOD

Tests

This investigation covered a Mach number range from 0.70 to 0.95 for all configurations except the standard and annular nozzles which were tested over a Mach number range of 0.70 to 1.05 and a range of total-pressure ratios from 1.0 (jet off) to approximately 4.5. The model angle of attack was maintained at 0° throughout the investigation. The average Reynolds number based on overall nacelle length was approximately 20×10^6. For the 8-lobe nozzle the secondary air pressure ratio was varied from about 0.6 to 1.2 for several primary jet pressure ratios.

L
8
5
0

Reduction of Data

The oscillograph records were read manually and the data converted to punch cards for reduction to standard coefficient form by machine computation. The coefficient of thrust minus drag was based on exit areas because of slight differences in exit areas between the configurations. The exit areas were corrected for expansion caused by the hot jet. The corrected jet areas are as follows:

Configuration	Jet exit area, sq ft
Standard	.0521
8-lobe	.0508
12-lobe	.0572
12-tube	.0562
Annular	.0496

Drag coefficients were based on maximum cross-sectional area of nacelle.

The thrust balance measured the propulsive force of the jet minus the external aerodynamic drag of the nozzle and some internal forces in the nacelle as shown in the schematic diagram of figure 5. Summing the axial forces on the thrust balance yields

$$F_{bal} = -p_1 A_{s1} - p_2(A_a - A_{s1}) + p_\infty A_a + F - D$$

It may be noted that the forces on only half the seal area are charged to the balance. Solving for the thrust minus drag yields

$$F - D = F_{bal} + A_{sl}(p_1 - p_2) + A_a(p_2 - p_\infty)$$

which indicates the method used in correcting the thrust balance readings for nacelle internal forces. In the case of the 8-lobe nozzles which included secondary air, the forces associated with the incoming secondary air were small enough to be neglected.

ACCURACY

The estimated accuracy of the data presented in this paper is as follows:

M	± 0.005
$p_{t,j}/p_o$	± 0.1
C_p	± 0.01
C_{F-D}	± 0.01

RESULTS AND DISCUSSION

Static Thrust Coefficients

In order to obtain an indication of the magnitude of the internal thrust losses for the various configurations, some data were taken under static conditions, that is, with tunnel off. For each configuration tested the measured and the ideal isentropic thrust coefficients are presented in figure 6 together with the ratios of measured to ideal thrusts. An indication of the relative internal efficiencies is shown in figure 7 where the thrust ratio of each configuration is compared with that of the standard nozzle. It may be noted that the thrust ratio F/F_i in figures 6 and 7 is equivalent to the velocity coefficient. For the sake of clarity the curves are divided into two groups and the standard nozzle curve is included in each group.

The 12-tube and the 12-lobe nozzles show a relatively high internal efficiency, even exceeding that of the standard nozzle at the higher pressure ratios. (See fig. 7.) A comparison of the annular nozzle with and without shroud indicates that the shroud acts as a thrust augmenter under static conditions. The curves for the 8-lobe nozzle indicate that the efficiency of this configuration is very sensitive to shroud length,

the shorter shroud being the more efficient under static conditions. The two points for secondary air $\left(p_{t,s}/p_\infty = 0.98\right)$ show that the efficiency is also sensitive to secondary air flow. The geometry of the 8-lobe nozzle base is such that the secondary air exit passages form a large proportion of the total base area; thus, the pressure increase in these passages (such as that caused by secondary air flow) increases the pressure acting on the base area and decreases base drag. With no secondary flow, the pressure in these passages was reduced by the ejector action of the primary jet as much as 5 pounds per square inch below atmospheric pressure $\left(p_{t,s}/p_\infty = 0.66\right)$ for the long shroud and up to about 0.3 pound per square inch $\left(p_{t,s}/p_\infty = 0.98\right)$ for the short shroud. This reduction indicates that the short shroud had the smaller base drag of the two and partly accounts for its superior performance.

The effect of secondary pressure ratio on thrust coefficients at a primary jet pressure ratio of 2.6 is shown in figure 8. Increase in secondary pressure ratio caused a slight increase in static thrust coefficient with about the same rate for both the short and long shroud lengths.

Thrust-Minus-Drag Coefficients

For the wind-tunnel tests the thrust balance was subjected to the additional force of afterbody aerodynamic drag. Since the thrust and drag components were not separable, a coefficient of thrust minus drag was used as a basis of performance comparison.

In figure 9 is presented thrust-minus-drag coefficient against jet pressure ratio at various Mach numbers for each configuration. It may be noted that the thrust-minus-drag coefficients are based on free-stream dynamic pressure instead of barometric pressure as in the case of the static tests. For each configuration, thrust minus drag increased almost linearly with increase in jet pressure ratio.

In order to form a basis for comparing the various configurations, a set of engine operating characteristics were assumed as shown in figure 10. The corrected weight flow ratio $\frac{w_s}{w_p}\sqrt{\frac{T_{t,s}}{T_{t,p}}}$ corresponding to the maximum secondary pressure ratio of figure 10 is about 0.04. Comparisons of thrust-minus-drag coefficients for these engine operating conditions are presented in figure 11; the configurations with no provision for secondary air, in figure 11(a) and those designed for secondary air, in figure 11(b). The standard nozzle curve is included on both sets of curves for comparison.

In figure 11(a) the 12-lobe and the 12-tube nozzles have almost similar performance characteristics, the 12-lobe nozzle showing a slight superiority. The lowest performance was indicated for the annular nozzles. In this case the shroud decreased the performance of the nozzle slightly, whereas under static conditions it had increased the performance very decidedly. (See fig. 7.)

In figure 11(b) the four configurations of the 8-lobe nozzle are compared with the standard nozzle. As in the static case, the short shroud showed a superiority over the long shroud. The use of secondary air increased the thrust minus drag in each case but produced a slightly more beneficial effect on the long shroud than on the short shroud. When the effect of secondary air on these data is evaluated, it should be noted that the secondary air, in this investigation, was supplied by an outside source. Therefore, the usual inlet and internal aerodynamic losses associated with a secondary air system do not appear in the thrust minus drag as used in this paper.

Figure 12 was included in this paper to give an indication of the effect of secondary air flow upon the thrust-minus-drag coefficients over a representative series of Mach numbers for primary jet pressure ratios of about 4.0 and 3.5 for each Mach number. For both the long and short shrouds, as indicated in figures 12(a) and 12(b), respectively, an increase in secondary pressure ratio increased the thrust-minus-drag coefficients fairly uniformly over the whole range of conditions.

Propulsive Thrust Loss

A further comparison of the various nozzle configurations on the basis of thrust loss compared with the standard nozzle at typical cruise conditions is shown in figure 13. The 12-lobe, the 12-tube, and the 8-lobe with long shroud configurations suffered losses of 5 to 7 percent as compared with the standard nozzle. The greatest losses (14 to 15 percent) occurred for the annular nozzle configurations. The smallest losses (about 1 percent) occurred for the 8-lobe nozzle with short shroud and secondary air. It should again be noted that the additional losses associated with taking aboard secondary air would increase the propulsive thrust loss of the 8-lobe nozzles. With the scheduled secondary air flow of these tests, this increase would be less than 1 percent and therefore would not change significantly the relative performance shown in the figure.

Effect of Pressure Ratio on Afterbody Surface

Pressure Distribution

A plot of pressure coefficients with axial location for three pressure ratios for the standard and 8-lobe nozzles are presented in figure 14. In general, the effect of increasing the pressure ratio is to increase the pressure on the surfaces near the jet exit. For the standard nozzle (fig. 14(a)) an effect of pressure ratio may be observed on the pressure distribution from the jet exit forward to the general vicinity of the peak pressures which occurred near the $x/l = 0.5$ to 0.6 stations. Forward of the peak pressure station the spread in the curves cannot be attributed to the effect of pressure ratio because the order is not consistent. For Mach numbers 0.70 and 0.82 there appears to be little or no difference between the curves for pressure ratios 3.0 and 4.0, the principal variation occurring between the curves for pressure ratios of 1.0 and 3.0, that is, between conditions of jet off and jet on. For a Mach number of 0.95, however, there is a decided difference between curves for pressure ratios 3.0 and 4.0.

The same general comments apply also to the pressure distributions of the 8-lobe nozzle. (See fig. 14(b).) However, the effects of pressure ratio for this case are smaller than those for the standard nozzle. This decrease in jet effect is probably caused by the shroud which partly shields the nearby surfaces from the influence of the jet. It should be noted that the four points representing pressure-coefficient distributions on the lobes are not a continuation of orifices on row $\phi = 90^\circ$ but are the averages of four orifices located on rows A, B, C, and D as indicated in figure 4(d). Also the orifices on the centerbody were not located on the 90° row but at the radial stations as shown in figure 4(d). The pressure distribution between the lobes indicated that there was no flow separation.

The pressures on the centerbody of the 8-lobe nozzle remained near ambient pressure for all jet-off conditions. At pressure ratio 2.7 (see fig. 14(b)), there is a strong pressure gradient where the pressure increased from a strong negative pressure near the jet exit to a strong positive pressure at the tip of the centerbody. For a pressure ratio of 4.0, the same strong pressure gradient existed from exit to tip, except for a break and sharp pressure reversal near the two middle tubes of the centerbody.

Variation of Pressure Drag With Mach Number

The variation of afterbody and base drag coefficients with Mach number for pressure ratios 1.0, 3.0, and 4.0 are presented in figure 15. For jet-off conditions (fig. 15(a)) the base drag was small for both

configurations and the 8-lobe nozzle with long shroud showed less afterbody drag than the standard nozzle at Mach numbers below the drag rise. This condition may have been caused by the smaller effective boattail angle of the 8-lobe nozzle. The drag rise for both nozzles occurred at a Mach number of about 0.88. It should be noted here that the base area of the 8-lobe nozzle was about 4 times that of the standard nozzle and is defined, as used in this paper, as the difference in area between that of the primary jet exit and the inside area of the shroud in the plane of the primary jet exit.

L
8
5
0

At a pressure ratio of 3.0 (fig. 15(b)) the standard nozzle afterbody drag has decreased from its jet-off value whereas the 8-lobe nozzle afterbody drag has increased. The cause of this increase was the large base drag (when no secondary air was used) which at some Mach numbers amounted to more than half of the afterbody drag. The boattail drag (which is the difference between base and afterbody drag) can be seen to be less than that of the standard nozzle.

At a pressure ratio of 4.0 (fig. 15(c)) the afterbody drags for both configurations show a decided decrease from those for a pressure ratio of 3.0. The base drag of the 8-lobe nozzle still amounted to half the afterbody drag for the lower Mach numbers. Extrapolation of the data indicates that the base drag of the 8-lobe nozzle would become zero at a pressure ratio of about 4.6 for Mach numbers 0.70 to 0.95. This condition would indicate that the afterbody drag of the 8-lobe nozzle would become very small at pressure ratios slightly higher than those covered in this investigation.

The triangular symbol indicates the effect of secondary air flow on the afterbody drag coefficient of the 8-lobe nozzle with long shroud. The decrease in drag indicates that the integrated pressure method of determining drag confirms the force method as to the beneficial effects of secondary air flow.

SUMMARY OF RESULTS

An investigation of the transonic performance characteristics of several noise-suppressor configurations was conducted in the Langley 16-foot transonic tunnel. The results of the investigation indicate the following:

1. The 8-lobe noise-suppressor nozzle with short shroud and secondary air flow evidenced the least aerodynamic penalty as compared with the standard nozzle.

2. The 12-lobe and 12-tube nozzles showed the least internal losses.

3. The ring shroud increased the thrust of the annular nozzle at static conditions but decreased the thrust minus drag slightly at transonic speeds.

4. The aerodynamic performance of the 8-lobe nozzle with short shroud was better than that for the 8-lobe nozzle with the long shroud. The performance with both shroud lengths was improved by secondary air flow.

5. Jet pressure ratio had more influence on the pressure distribution of the standard nozzle than that of the 8-lobe nozzle. Increase in pressure ratio increased the pressure on those parts of the afterbodies nearest the jet exits for both standard and 8-lobe nozzles and resulted in a decrease in afterbody drag.

L
8
5
0

Langley Research Center,
National Aeronautics and Space Administration,
Langley Field, Va., March 1, 1960.

REFERENCES

1. Ciepluch, Carl C., North, Warren J., Coles, Willard D., and Antl, Robert J.: Acoustic, Thrust, and Drag Characteristics of Several Full-Scale Noise Suppressors for Turbojet Engines. NACA TN 4261, 1958.

2. North, Warren J.: Transonic Drag of Several Jet-Noise Suppressors. NACA TN 4269, 1958.

3. Coles, Willard D., Mihaloew, John A., and Callaghan, Edmund E.: Turbojet Engine Noise Reduction With Mixing Nozzle-Ejector Combinations. NACA TN 4317, 1958.

4. Runckel, Jack F., and Swihart, John M.: A Hydrogen Peroxide Hot-Jet Simulator for Wind-Tunnel Tests of Turbojet-Exit Models. NASA MEMO 1-10-59L, 1959.

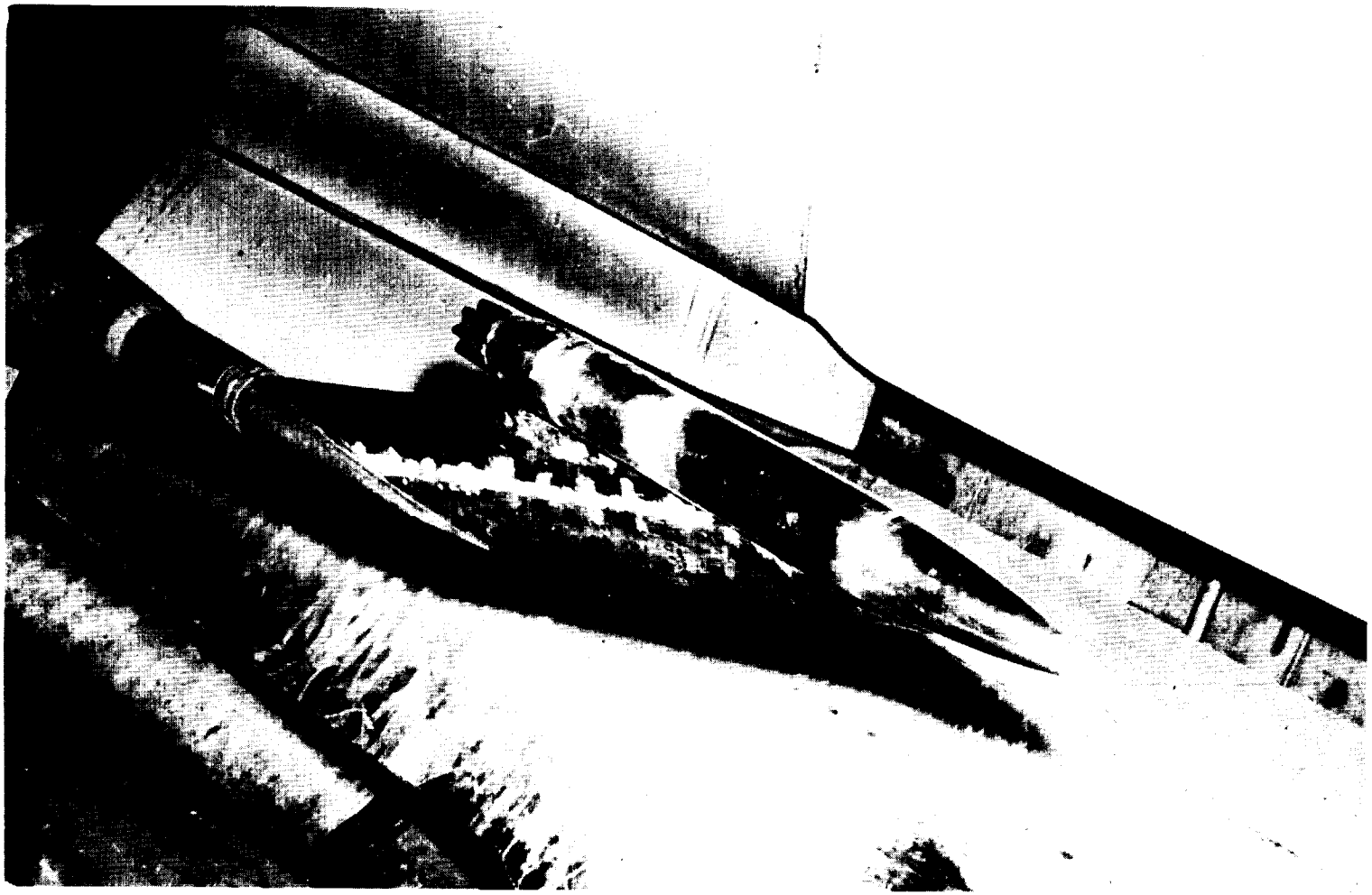

L-58-1102a

Figure 1.- Eight-lobe nozzle mounted on pylon-nacelle model in Langley 16-foot transonic tunnel.

FOREBODY ORDINATES			
Station, x	Radius, r	Station, x	Radius, r
2.000	0.490	20.000	3.080
5.000	1.140	20.900	3.127
8.000	1.700	23.500	3.220
11.000	2.175	26.000	3.250
14.000	2.565	51.875	3.250
17.000	2.865		

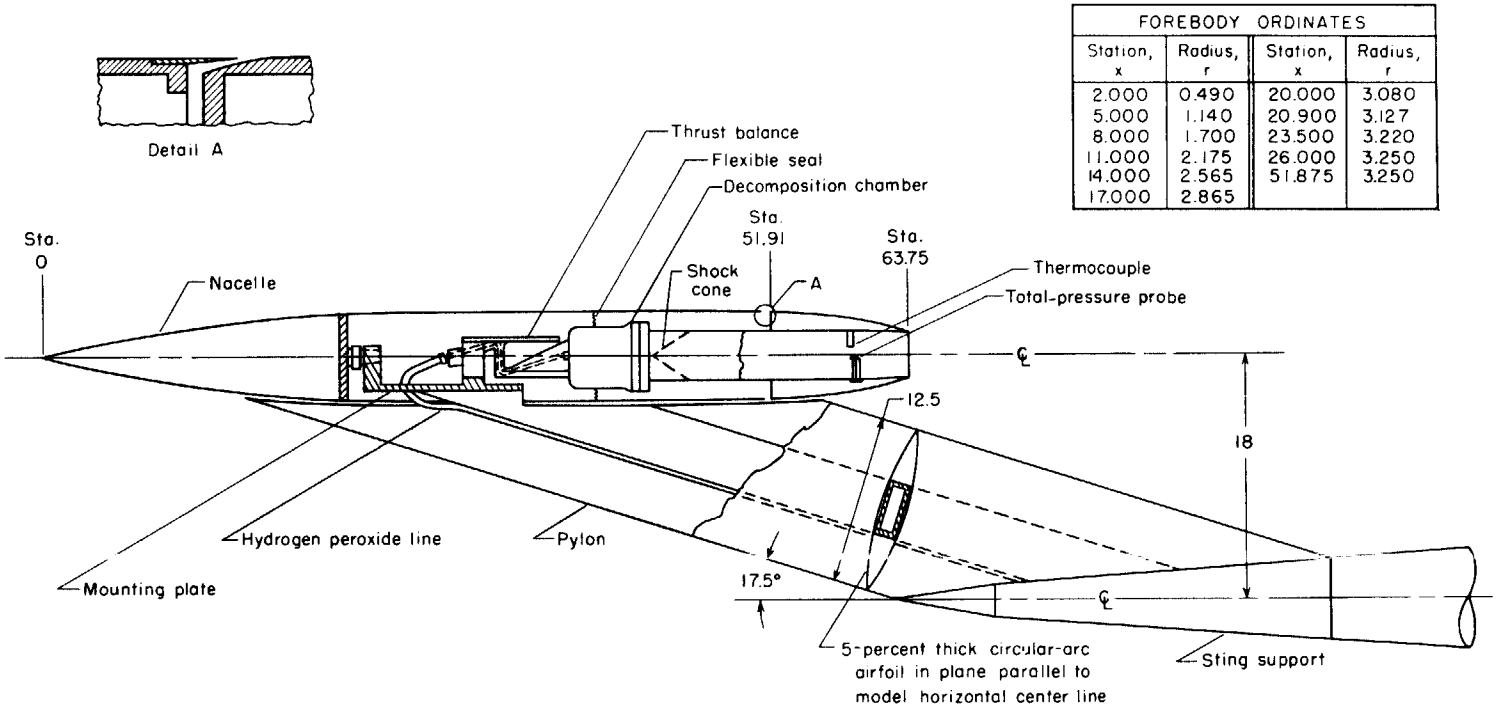

Figure 2.- Sketch of pylon-supported nacelle model. All dimensions are in inches.

Static Orifice Locations			
x	x/l	r	Row
0.0	0.0	3.25	ø = 0°, 45°, 90°, 135°, 165°
1.0	.08	3.24	
2.68	.23	3.20	
4.36	.37	3.14	
5.23	.44	3.11	
5.98	.51	3.04	ø = 0°, 45°, 90°, 135°, 165°, 180°
6.74	.57	2.93	
7.47	.63	2.78	
8.21	.69	2.59	
9.67	.82	2.22	
10.41	.88	2.00	
11.84	1.00	1.63	

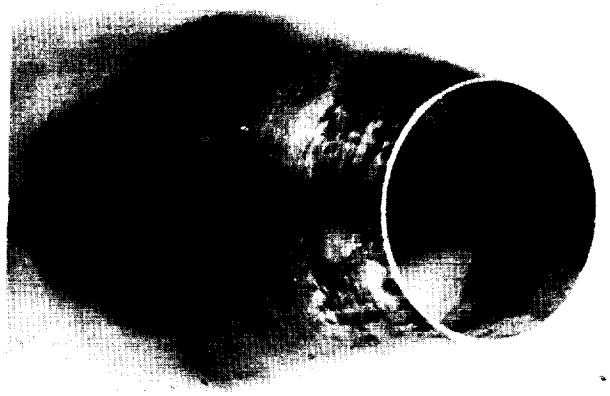

L-59-5370

L-850

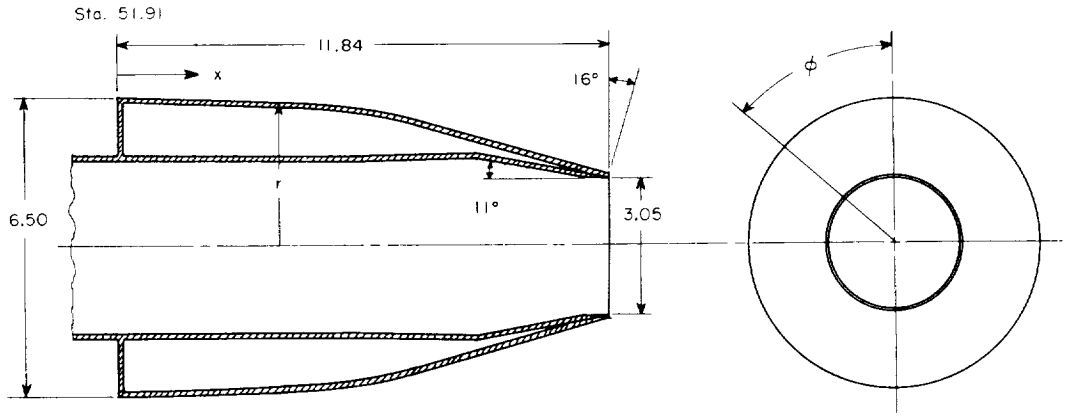

Figure 3.- Standard nozzle. All dimensions are in inches.

Afterbody Coordinates

x	r
1.03	3.25
2.65	3.21
3.37	3.19
4.10	3.16
4.86	3.08
5.61	2.89
6.30	2.67
7.01	2.42
7.94	2.13
8.26	2.02

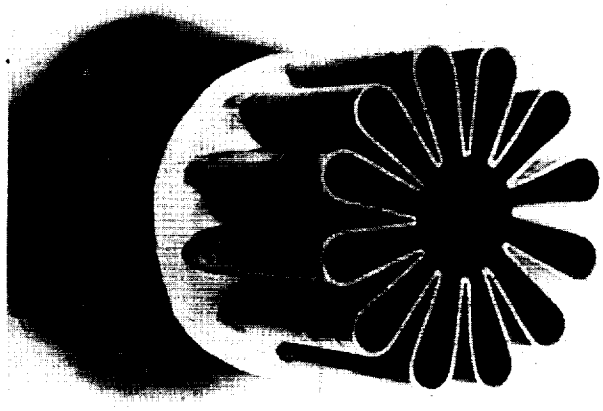

L-59-5368

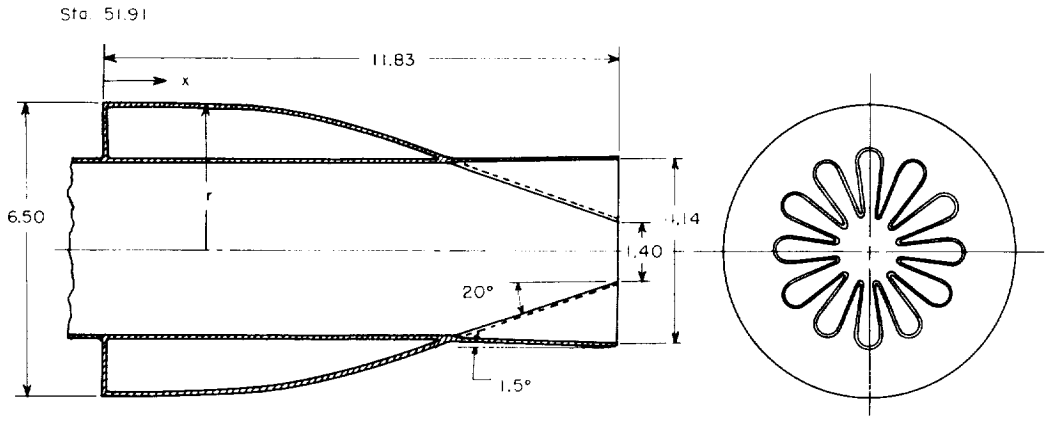

(a) Twelve-lobe nozzle.

Figure 4.- Noise-suppressor configurations. All dimensions are in inches.

L-850

Afterbody Coordinates

x	r
0.98	3.24
2.60	3.22
3.60	3.16
4.33	3.09
5.07	2.98
5.82	2.80
6.54	2.60
7.27	2.39
7.67	2.25
8.75	1.93

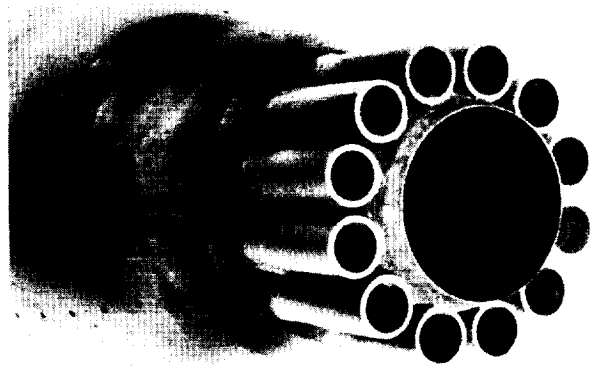

L-59-5367

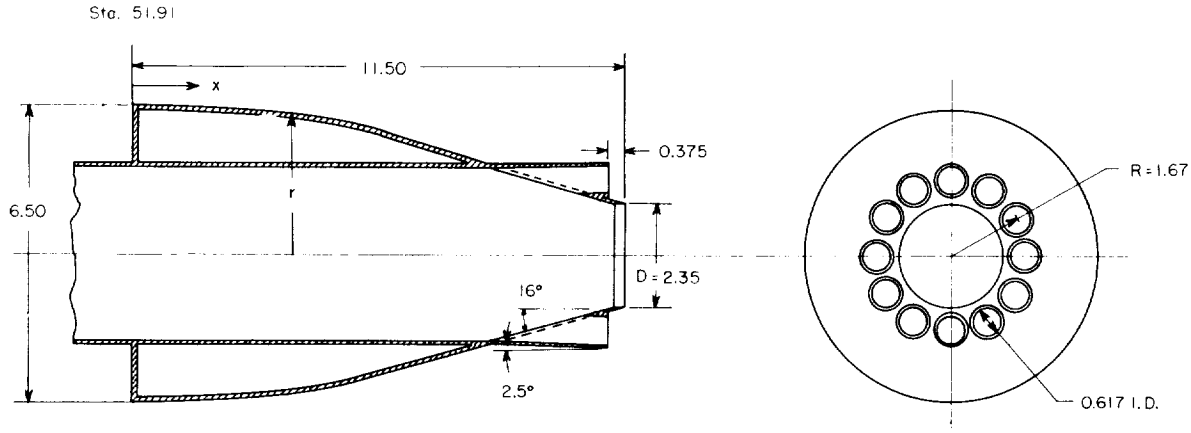

(b) Twelve-tube nozzle.

Figure 4.- Continued.

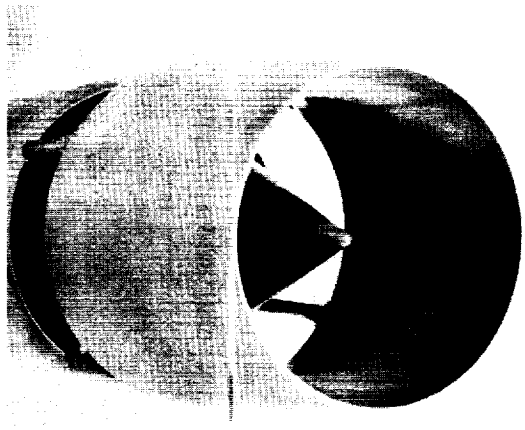

L-59-5202

Afterbody Coordinates

Shroud		
x_1	r_1	r_2
0.0	3.200	3.200
.2	3.010	3.256
.4	2.934	3.252
.6	2.871	3.241
1.0	2.779	3.210
1.4	2.715	3.177
2.0	2.652	3.117
3.0	2.610	3.012
4.0	2.600	2.906
5.0	2.600	2.800
6.5	2.600	2.640

Cone	
x	r
0.0	2.515
.5	2.405
1.21	1.985
Conical	
7.9	.070

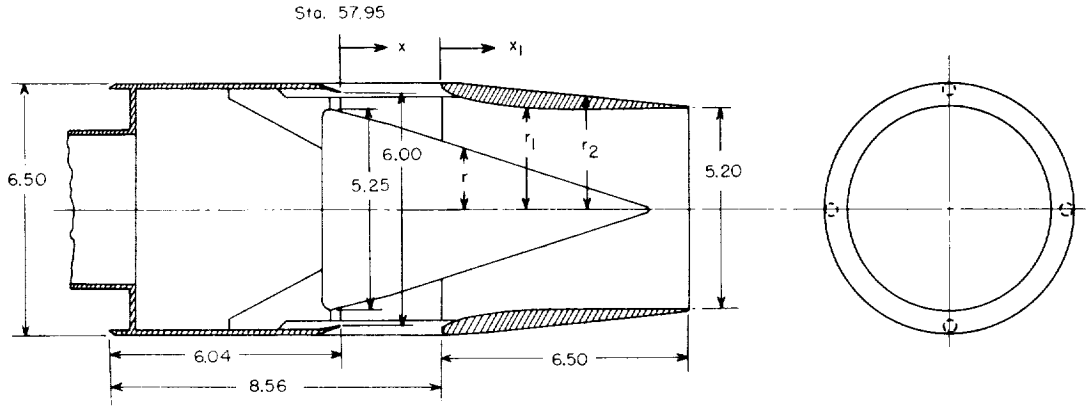

(c) Annular nozzle with shroud.

Figure 4.- Continued.

Static Orifice Locations			
x	x/l	r	Row
1.00	0.08	3.24	ϕ = 0°, 45°, 90° 135°, 165°
2.62	.22	3.24	
3.37	.28	3.24	
4.11	.35	3.22	
4.86	.41	3.19	
5.61	.47	3.10	ϕ = 0°, 45°, 90° 135°, 165°, 180°
6.36	.54	2.99	
7.11	.60	2.84	
Lobes			
x	x/l	r	Row
8.70	0.73	——	A, B, C, and D
9.88	.83	——	
10.91	.92	——	
11.99	1.01	——	
Centerbody			
x	x/l	r	Row
12.82	1.08	——	ϕ = 0°
13.27	1.12	——	ϕ = 315°
13.70	1.16	——	ϕ = 270°
14.10	1.19	——	ϕ = 225°

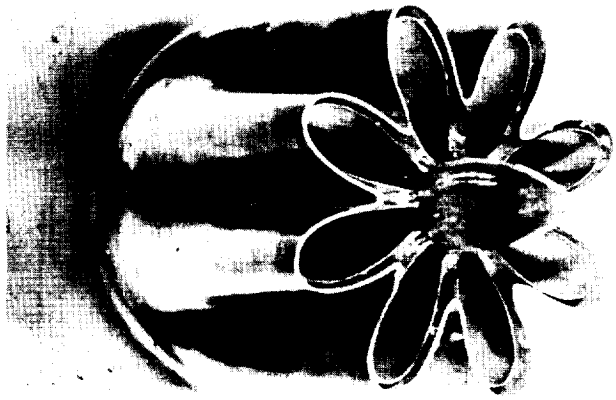

L-59-5369

Effective Values	L/d_p	d_s/d_p
Long shroud	0.277	1.13
Short shroud	.043	1.13

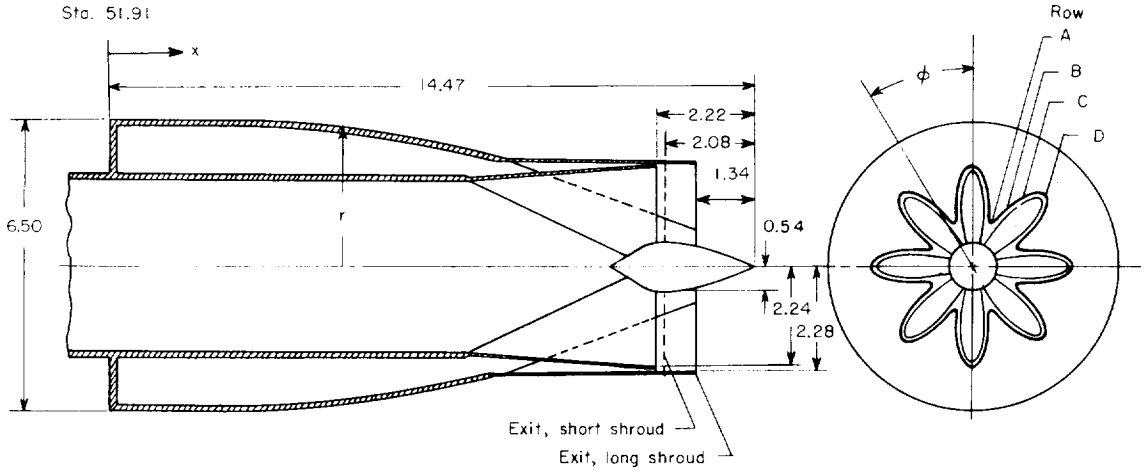

(d) Eight-lobe nozzle with shroud.

Figure 4.- Concluded.

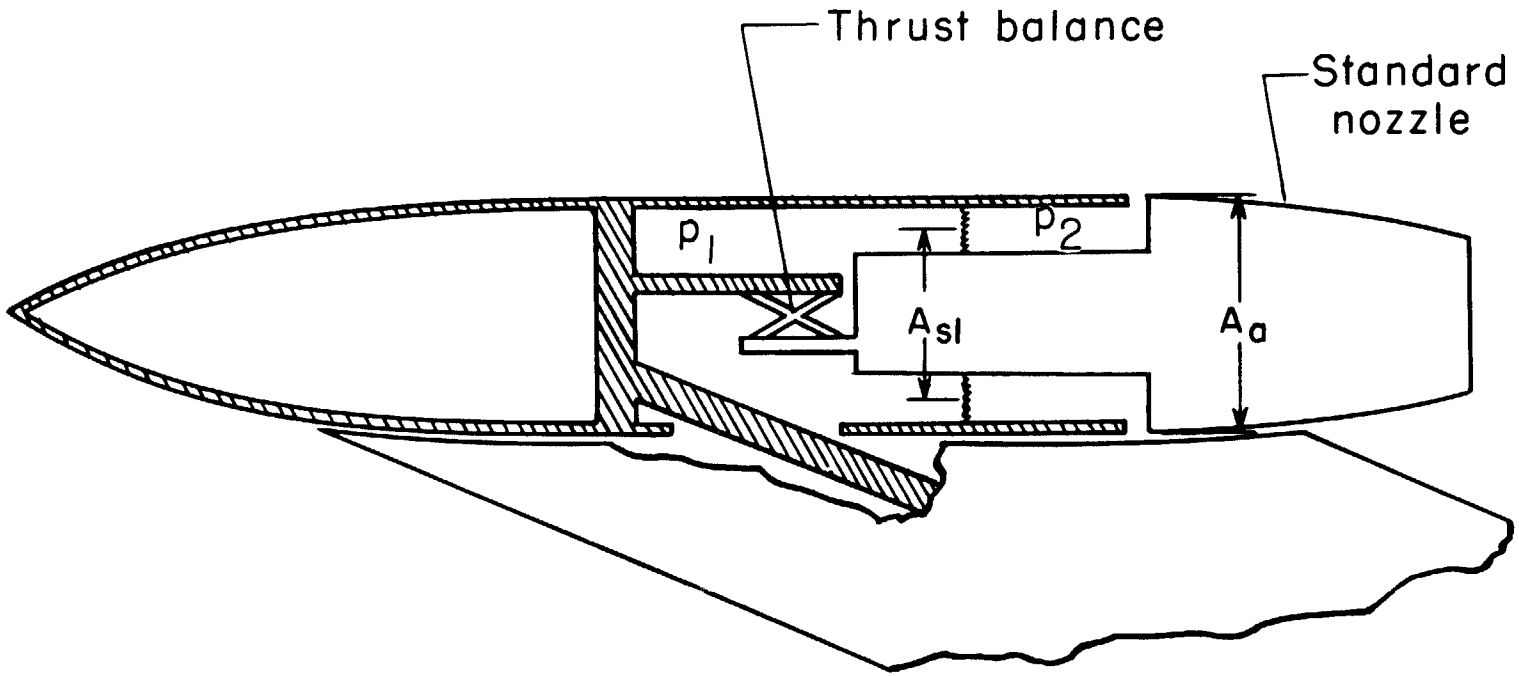

Figure 5.- Schematic diagram of measuring system.

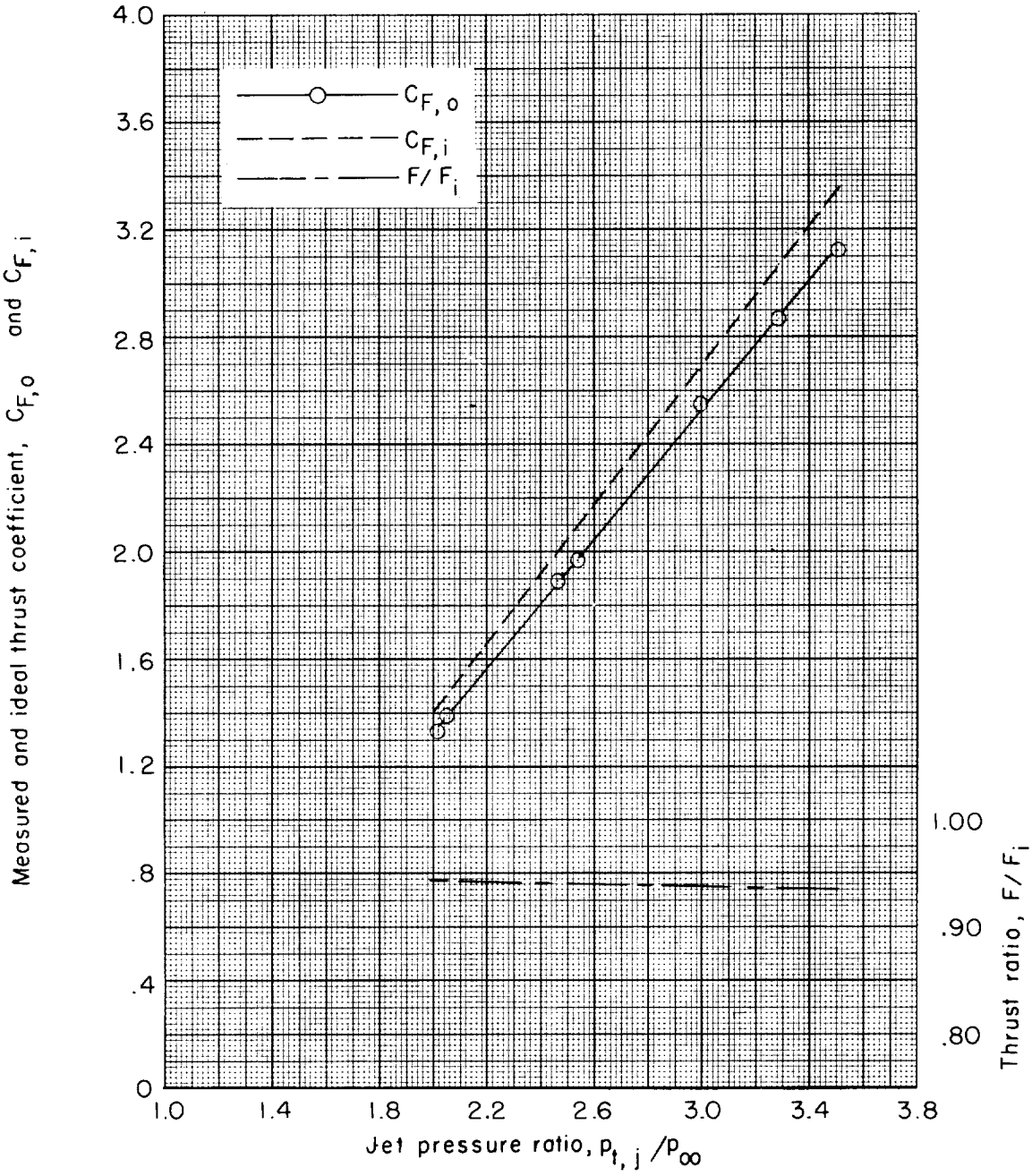

(a) Standard nozzle.

Figure 6.- Variation of static thrust coefficient with jet pressure ratio for the test configurations.

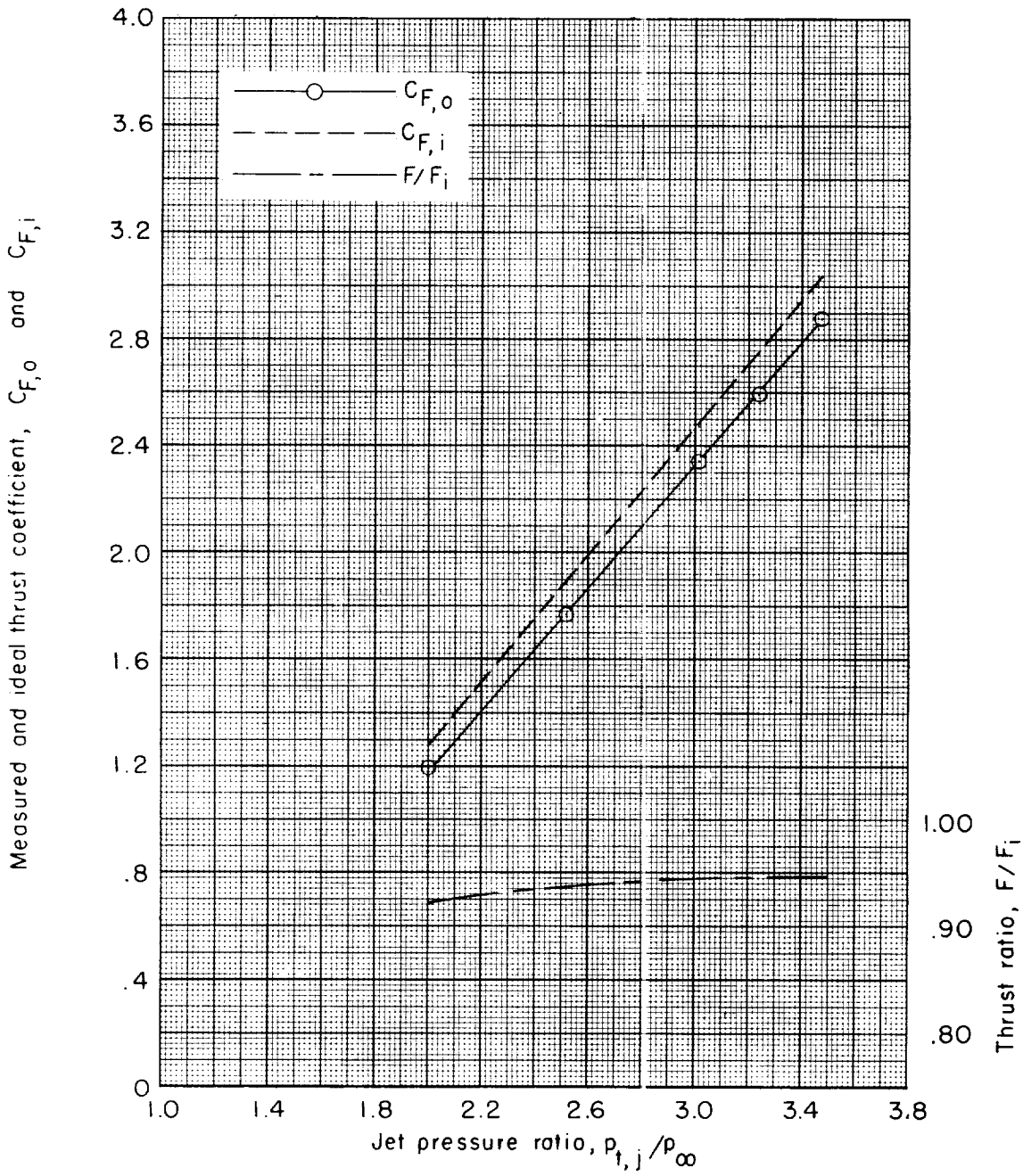

(b) Twelve-tube nozzle.

Figure 6.- Continued.

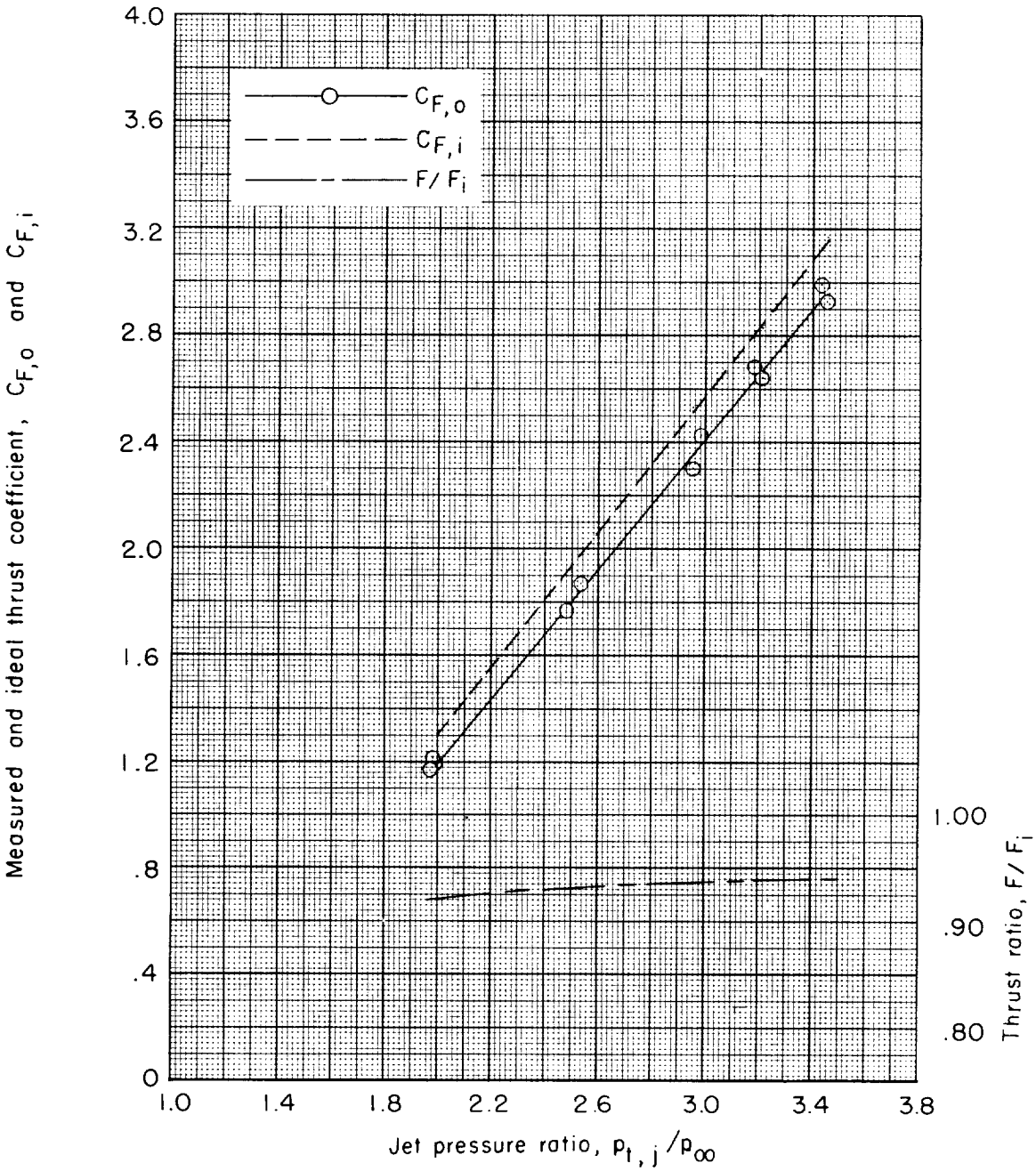

(c) Twelve-lobe nozzle.

Figure 6.- Continued.

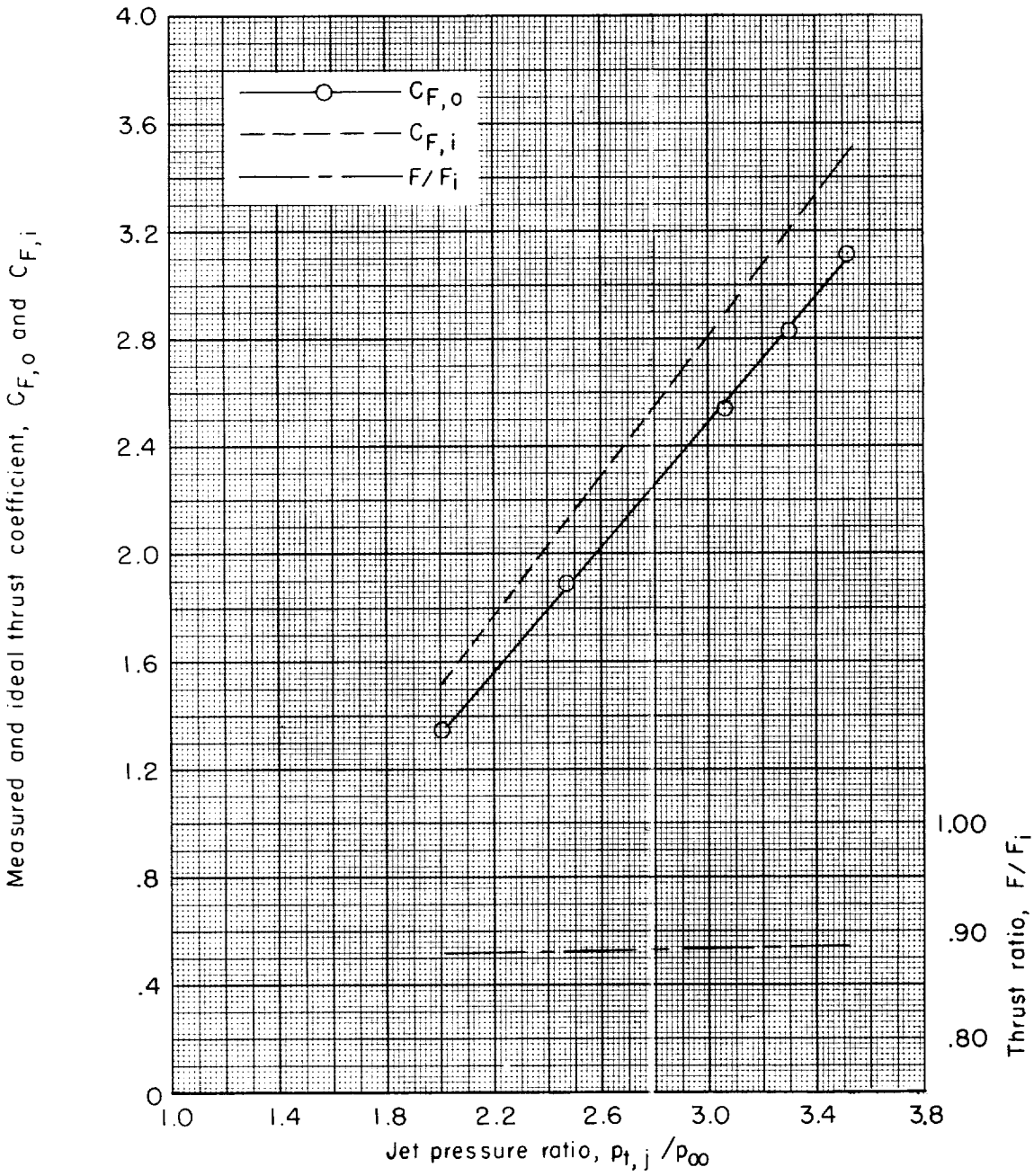

(d) Eight-lobe nozzle with short shroud. $L/d_e = 0.044$.

Figure 6.- Continued.

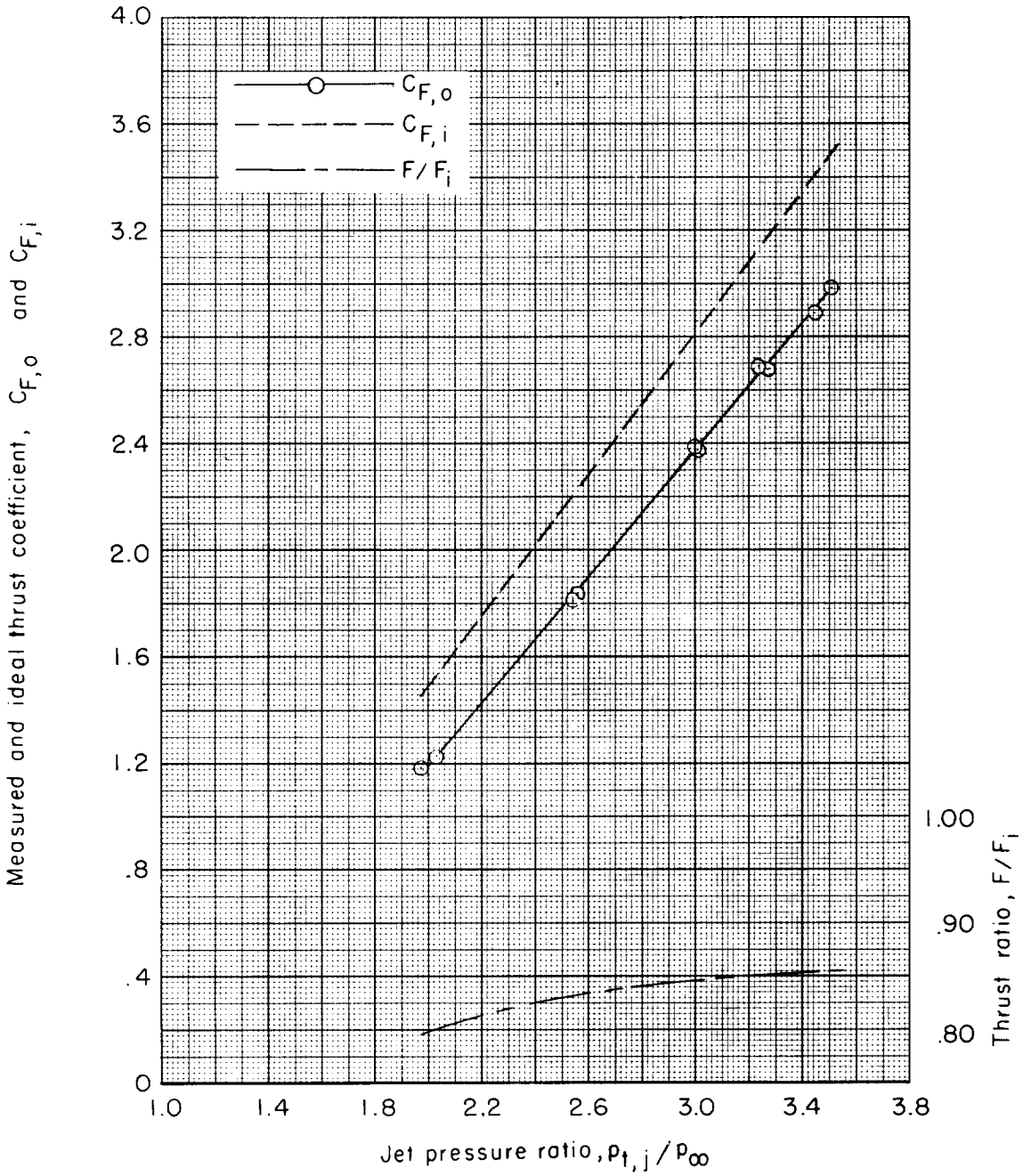

(e) Eight-lobe nozzle with long shroud. $L/d_e = 0.284$.

Figure 6.- Continued.

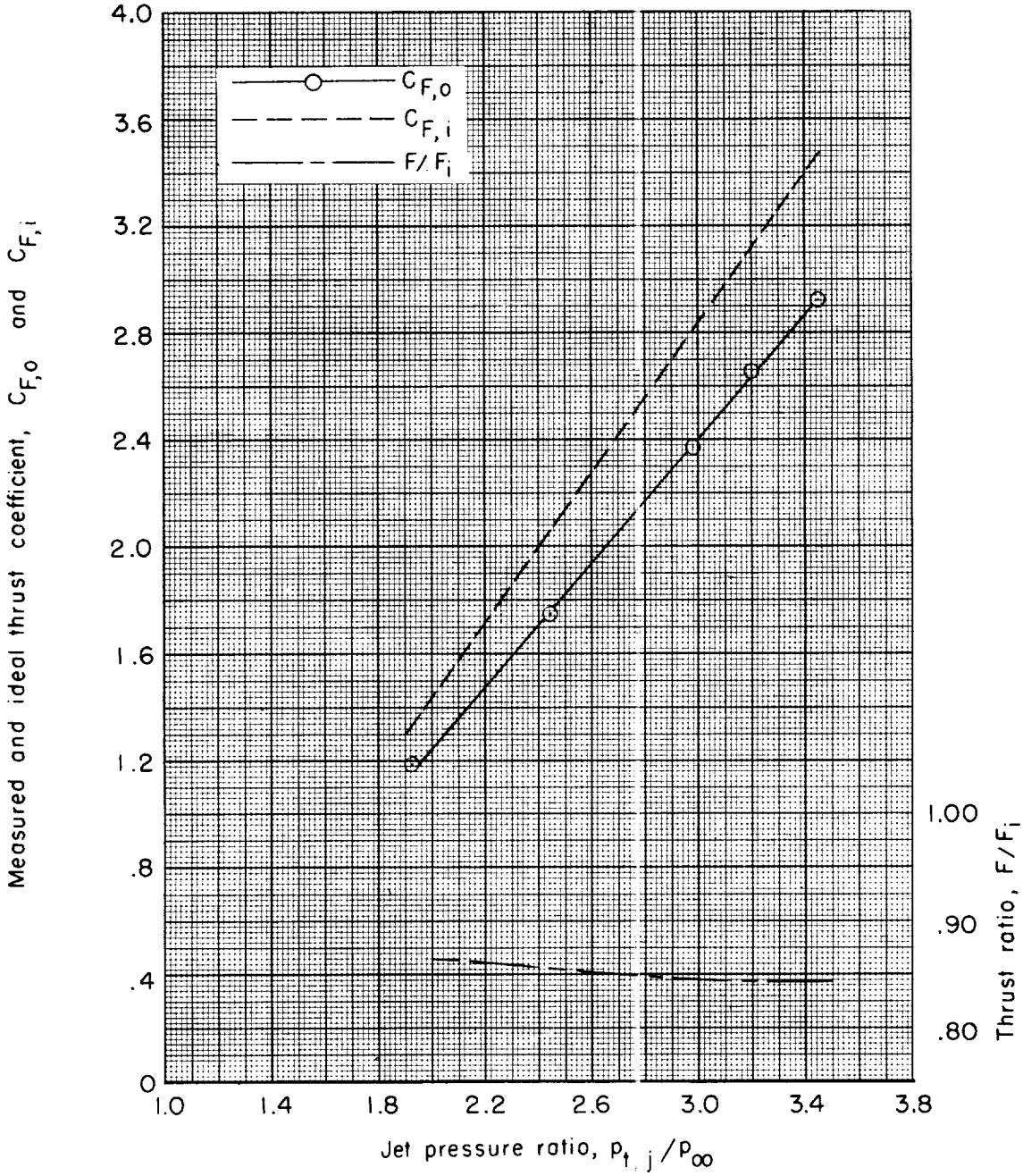

L-850

(f) Annular nozzle.

Figure 6.- Continued.

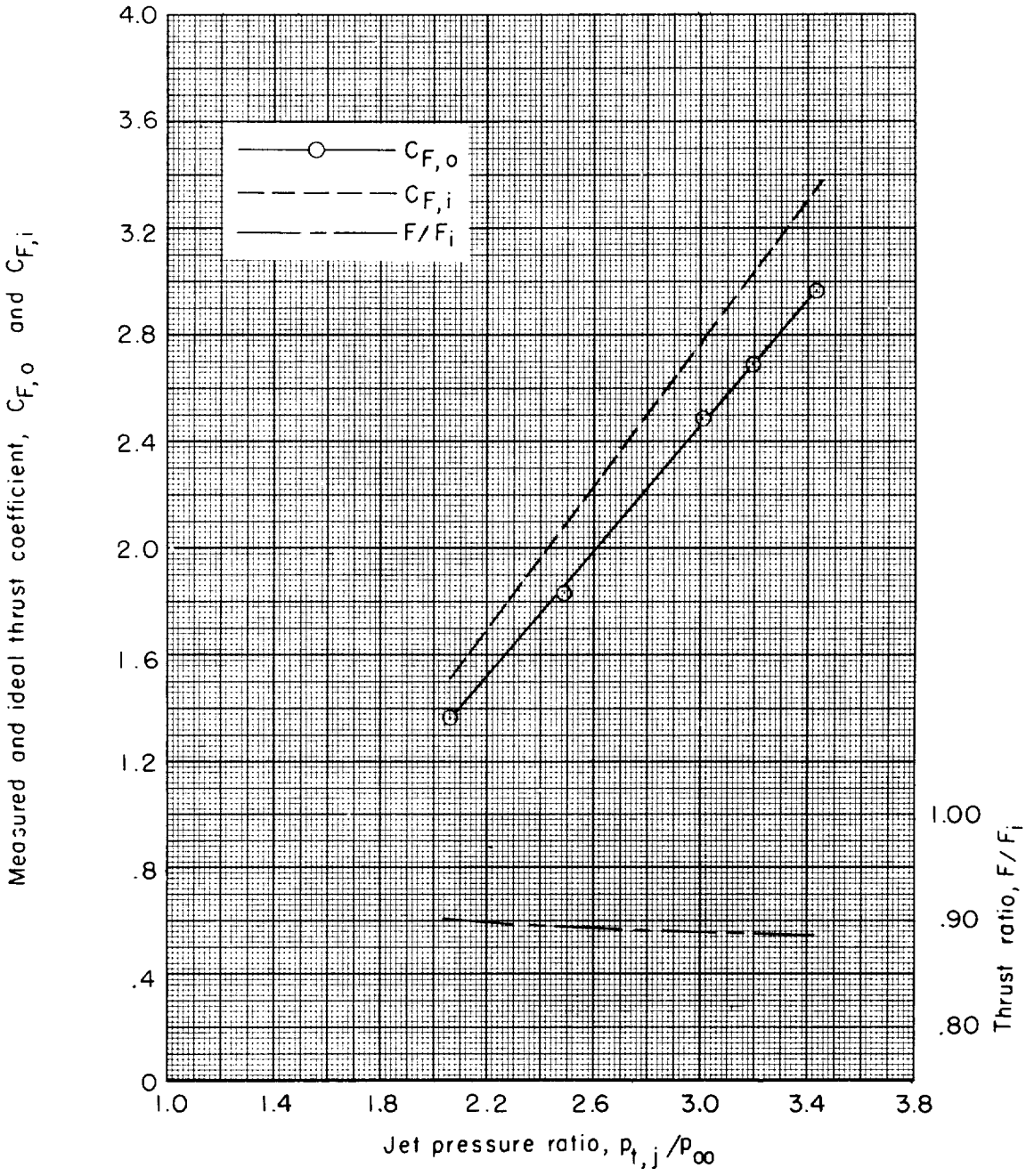

(g) Annular nozzle with shroud.

Figure 6.- Concluded.

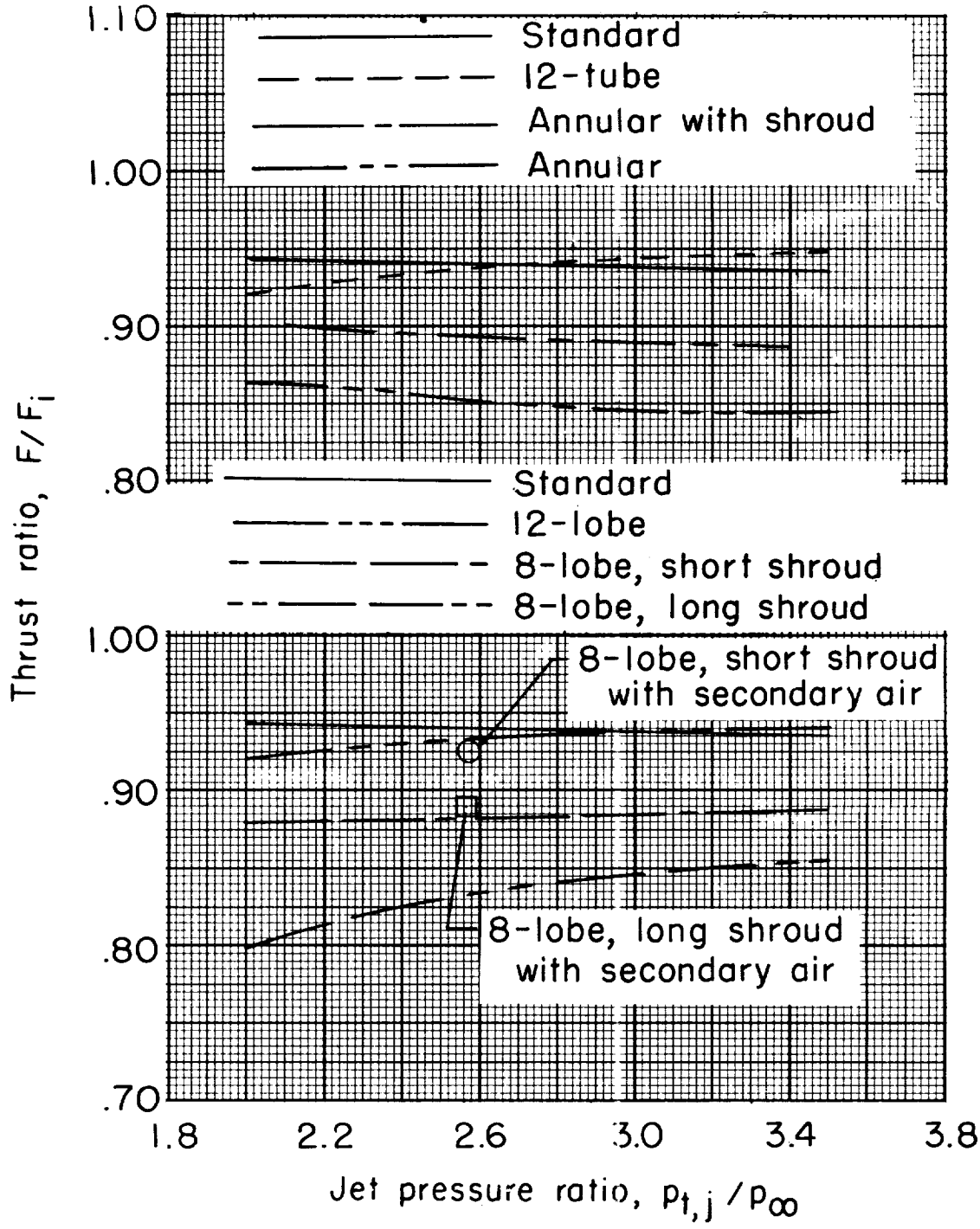

Figure 7.- Comparison of static-thrust ratios of noise-suppressor configurations with standard nozzle.

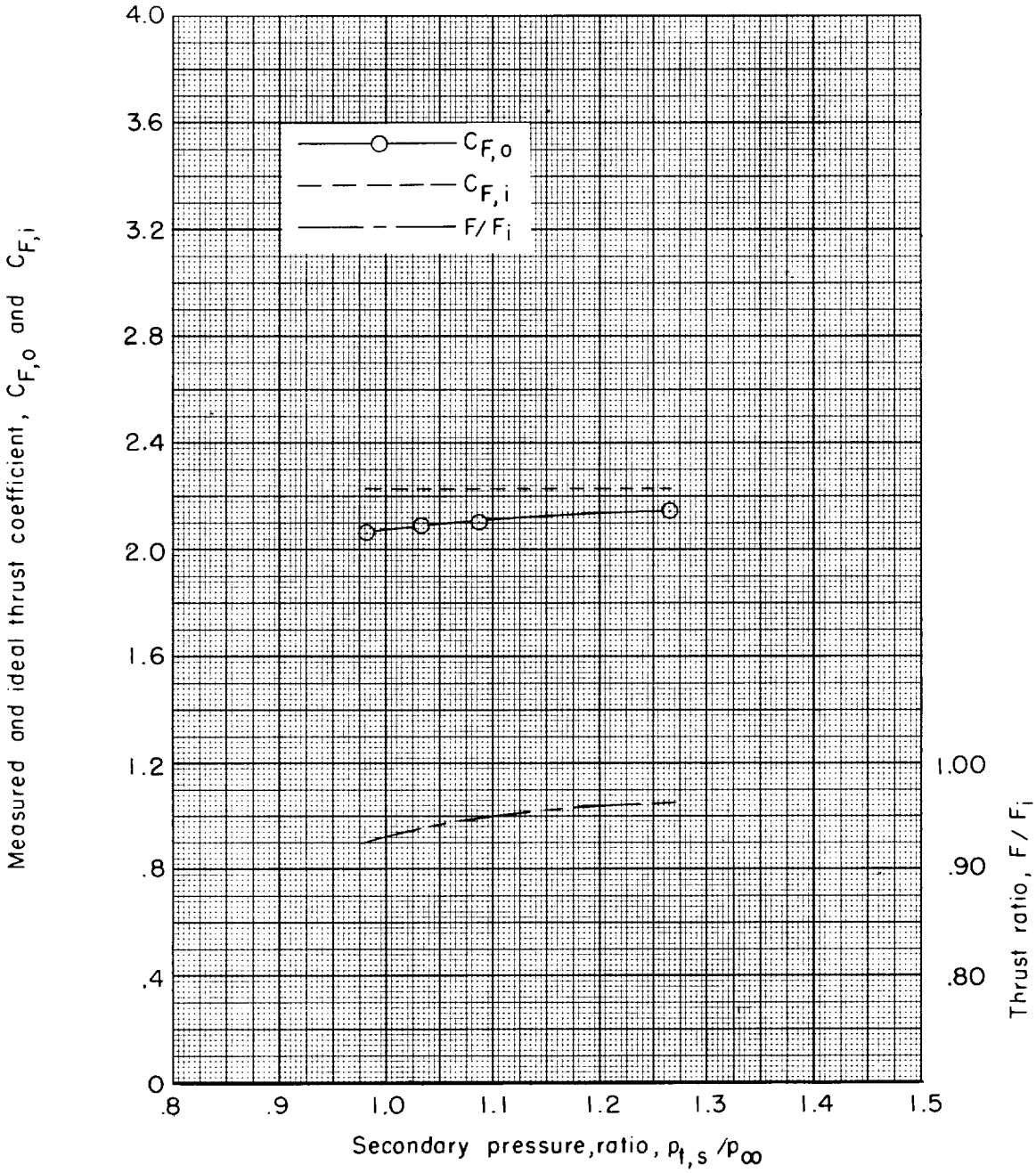

(a) Short shroud. $L/d_e = 0.044$.

Figure 8.- Variation of static thrust coefficient with secondary pressure ratio for 8-lobe nozzle with shroud. $p_{t,j}/p_\infty = 2.57$.

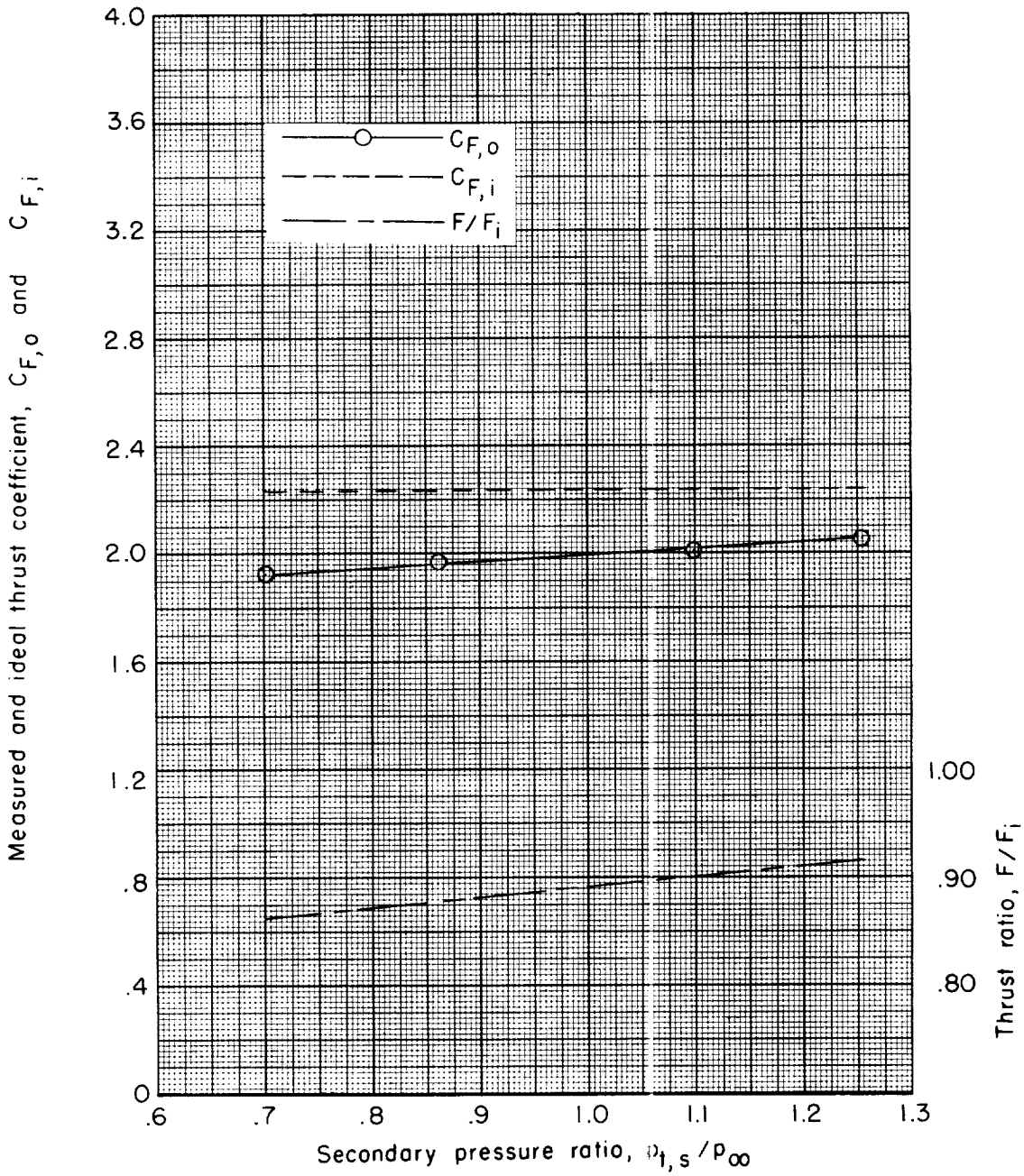

(b) Long shroud. $L/d_e = 0.284$.

Figure 8.- Concluded.

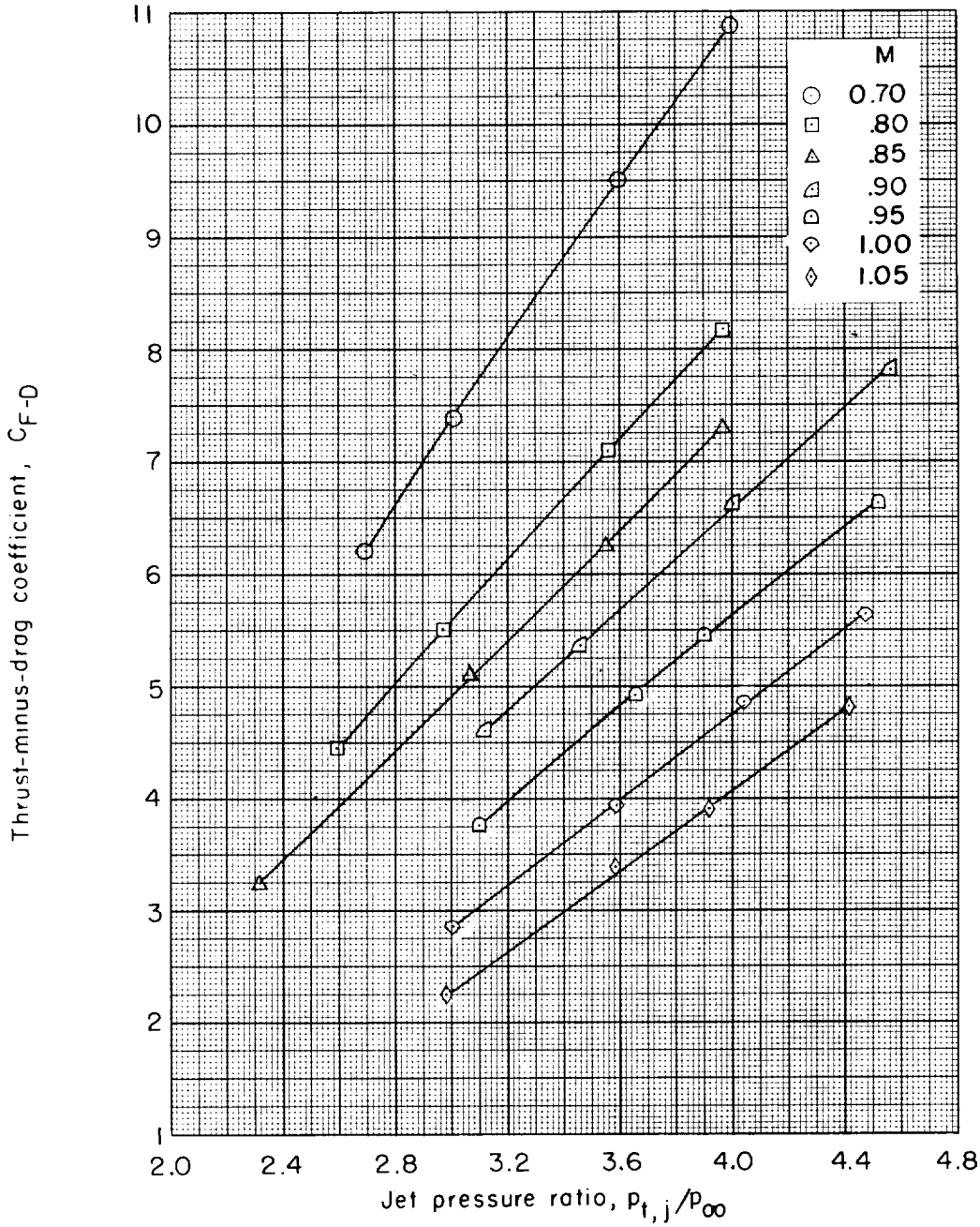

(a) Standard nozzle.

Figure 9.- Variation of thrust-minus-drag coefficient with jet pressure ratio and Mach number.

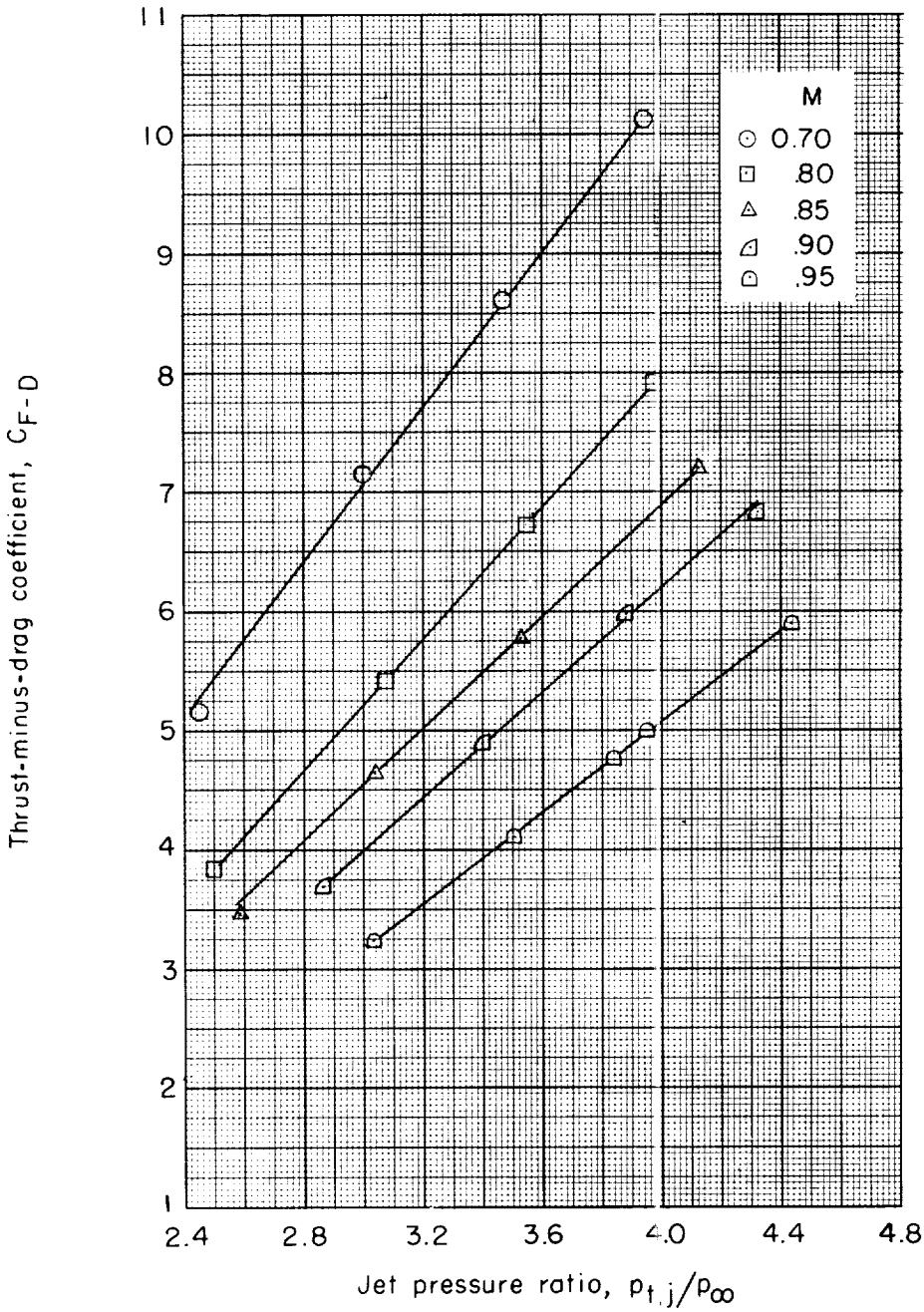

(b) Twelve-tube nozzle.

Figure 9.- Continued.

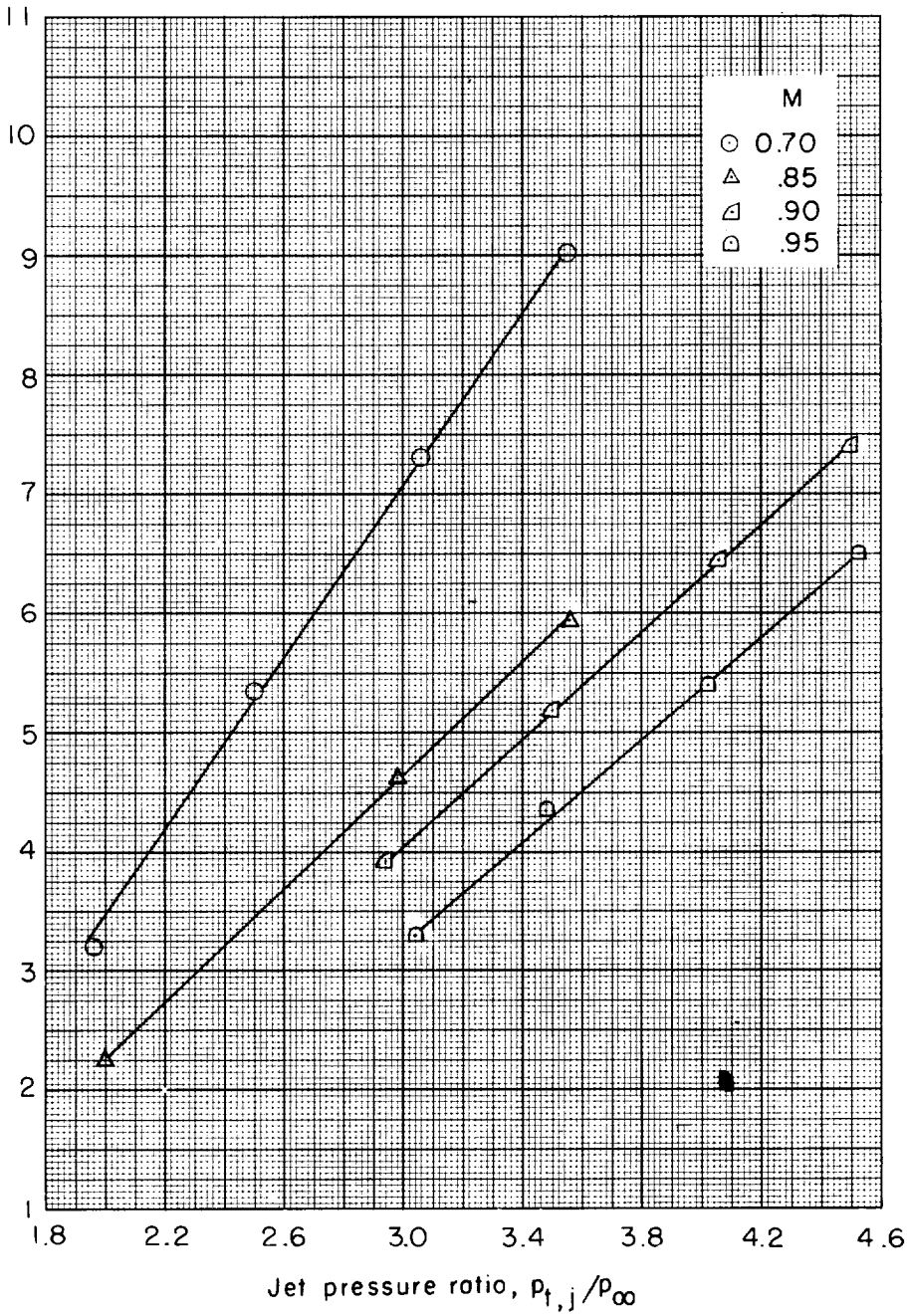

(c) Twelve-lobe nozzle.

Figure 9.- Continued.

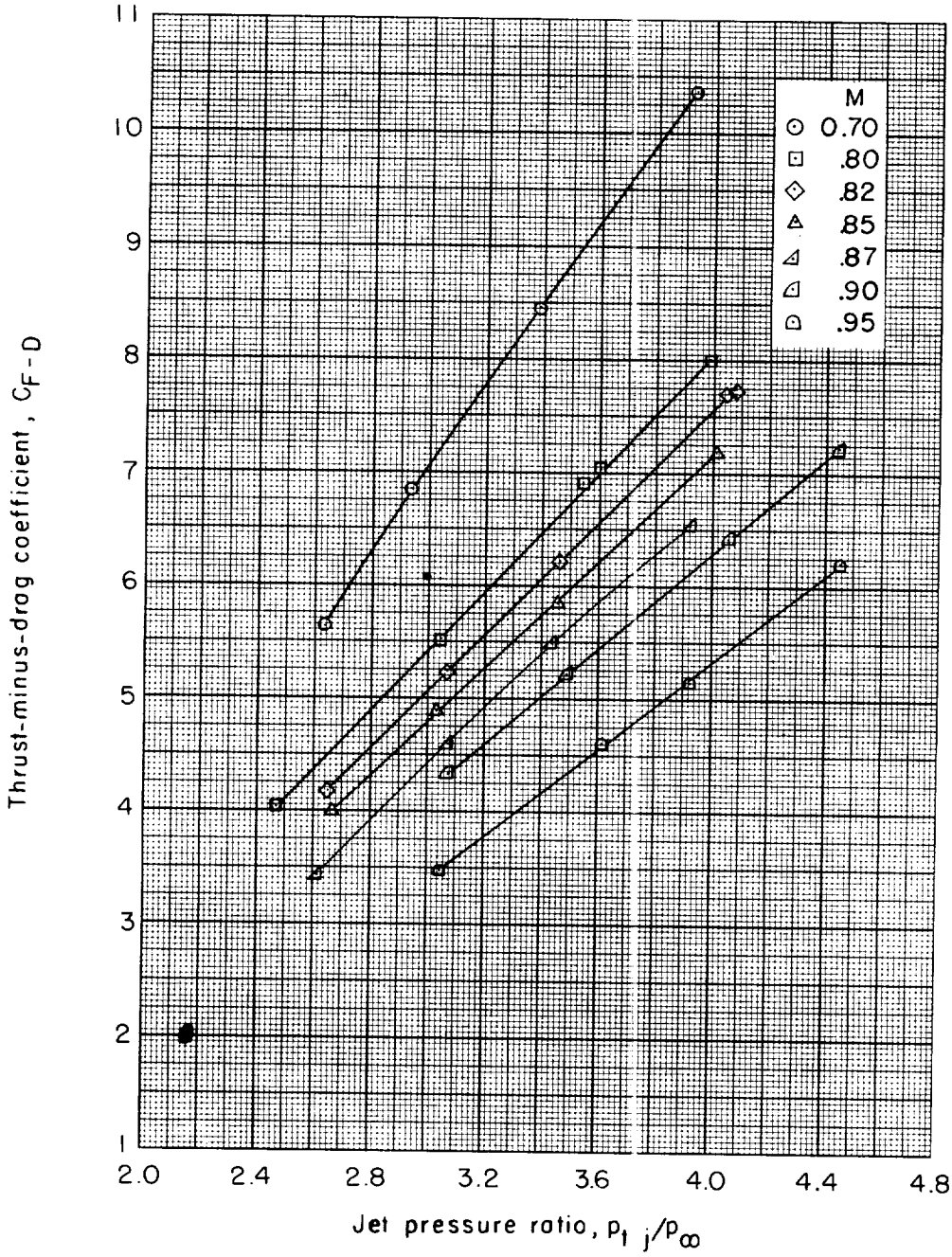

(d) Eight-lobe nozzle with short shroud. $L/d_e = 0.044$.

Figure 9.- Continued.

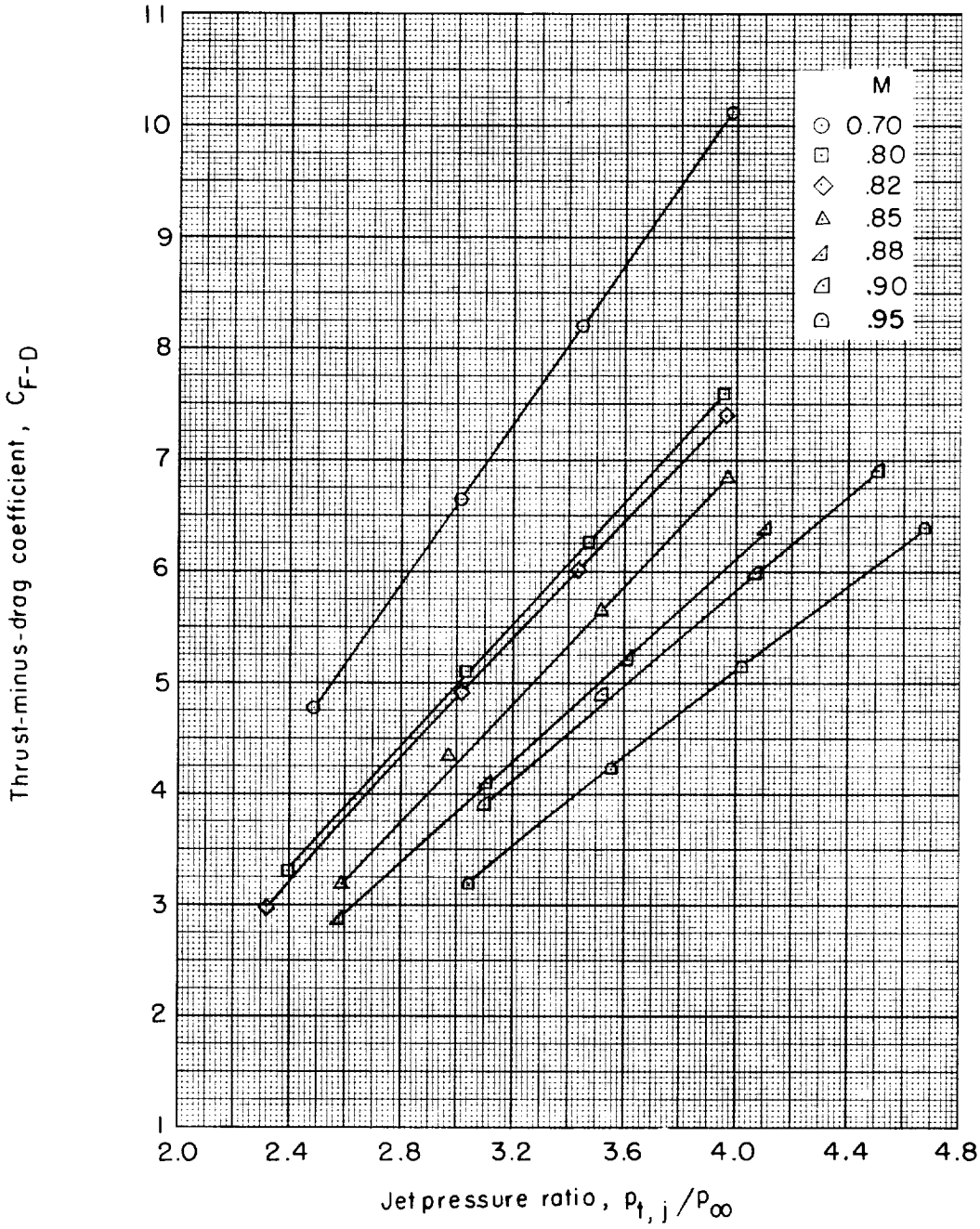

(e) Eight-lobe nozzle with long shroud. $L/d_e = 0.284$.

Figure 9.- Continued.

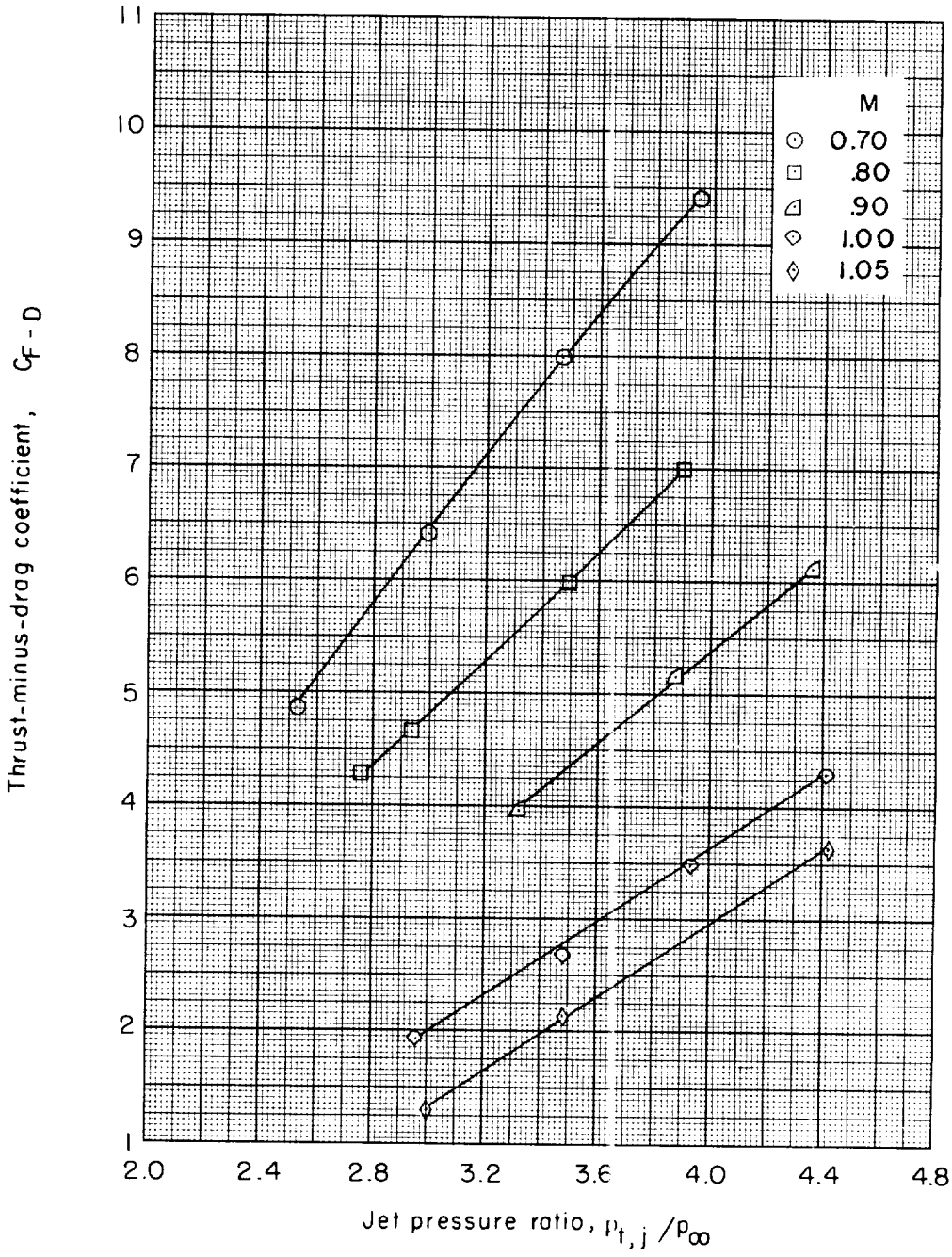

(f) Annular nozzle.

Figure 9.- Continued.

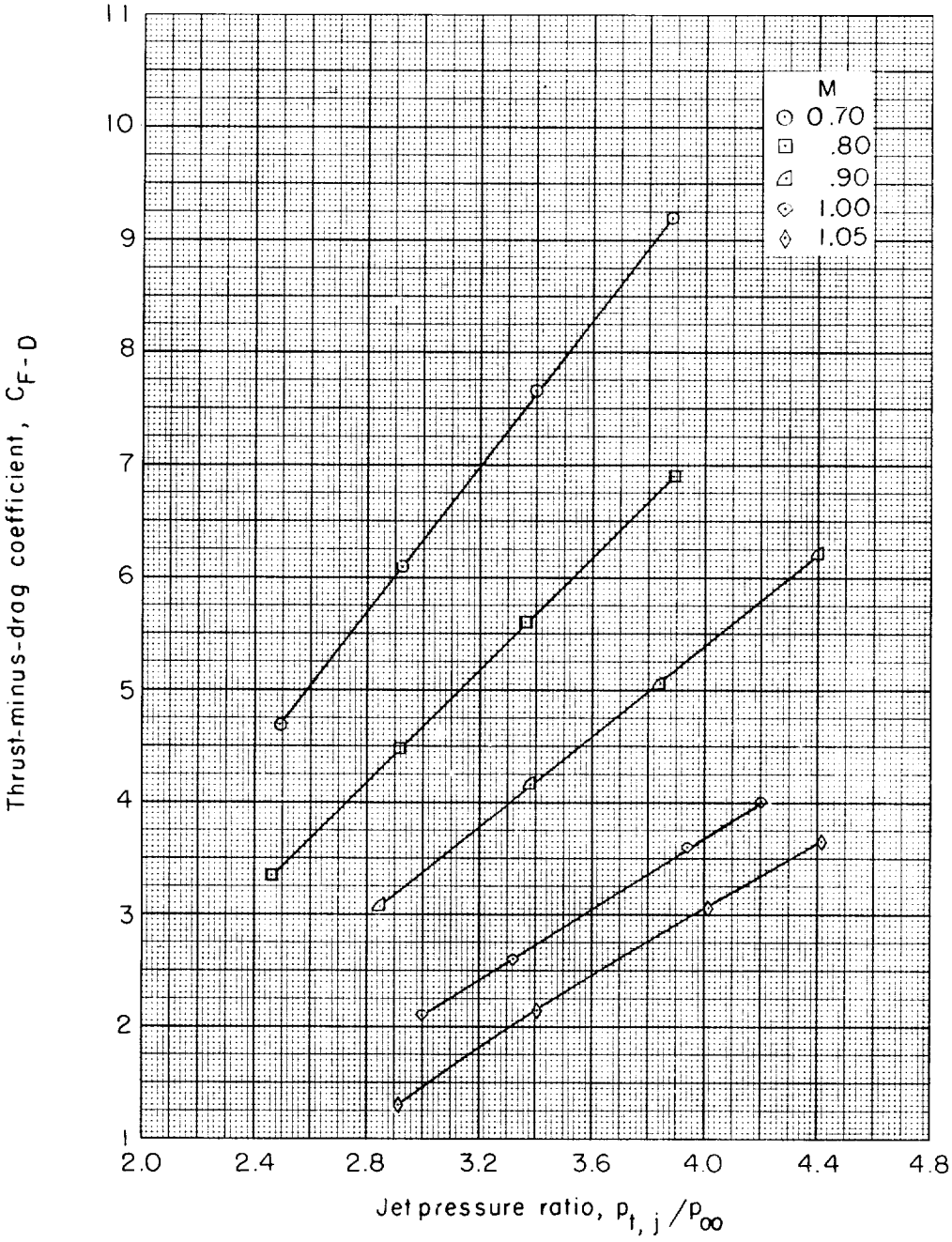

(g) Annular nozzle with shroud.

Figure 9.- Concluded.

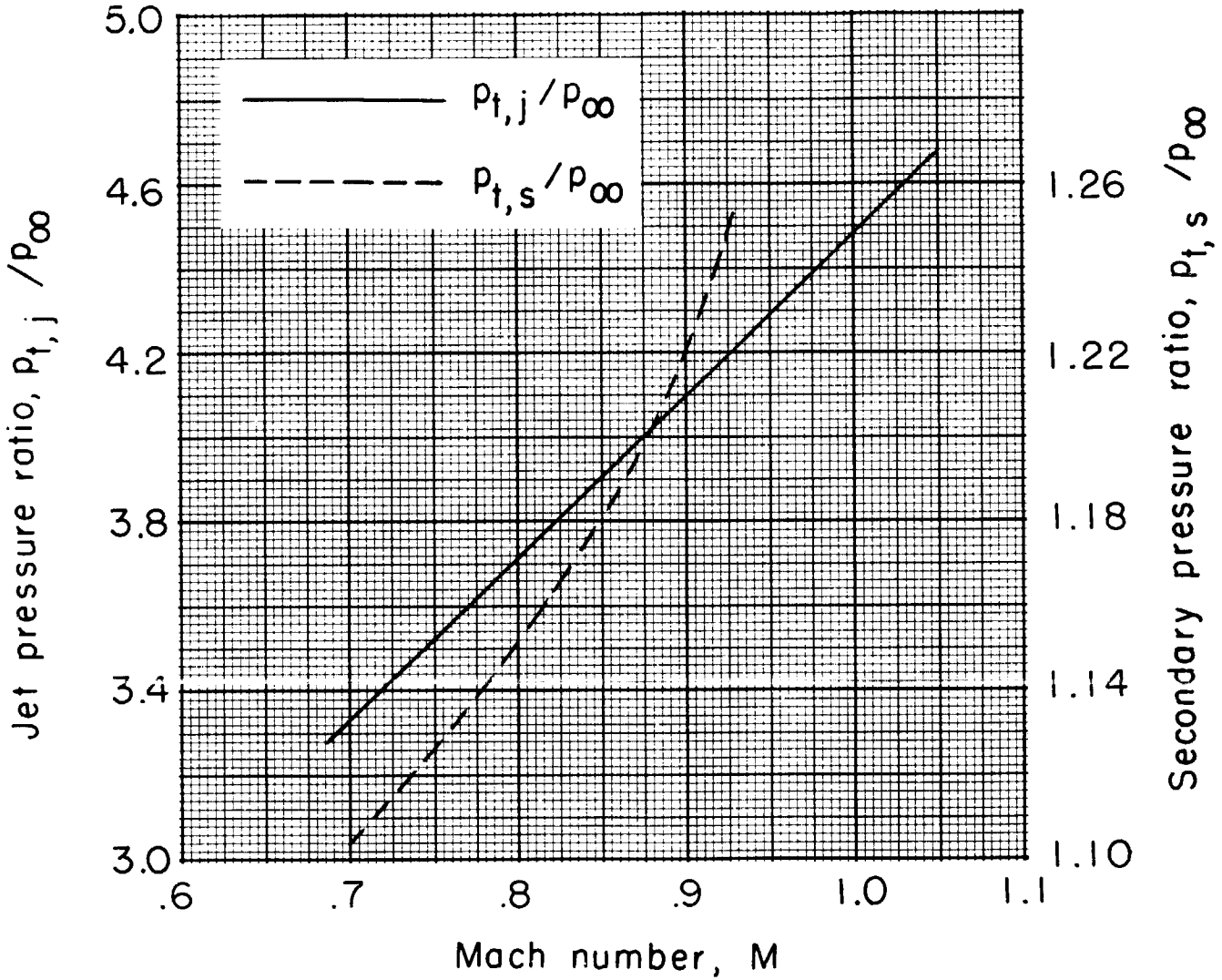

Figure 10.- Assumed engine operating characteristics.

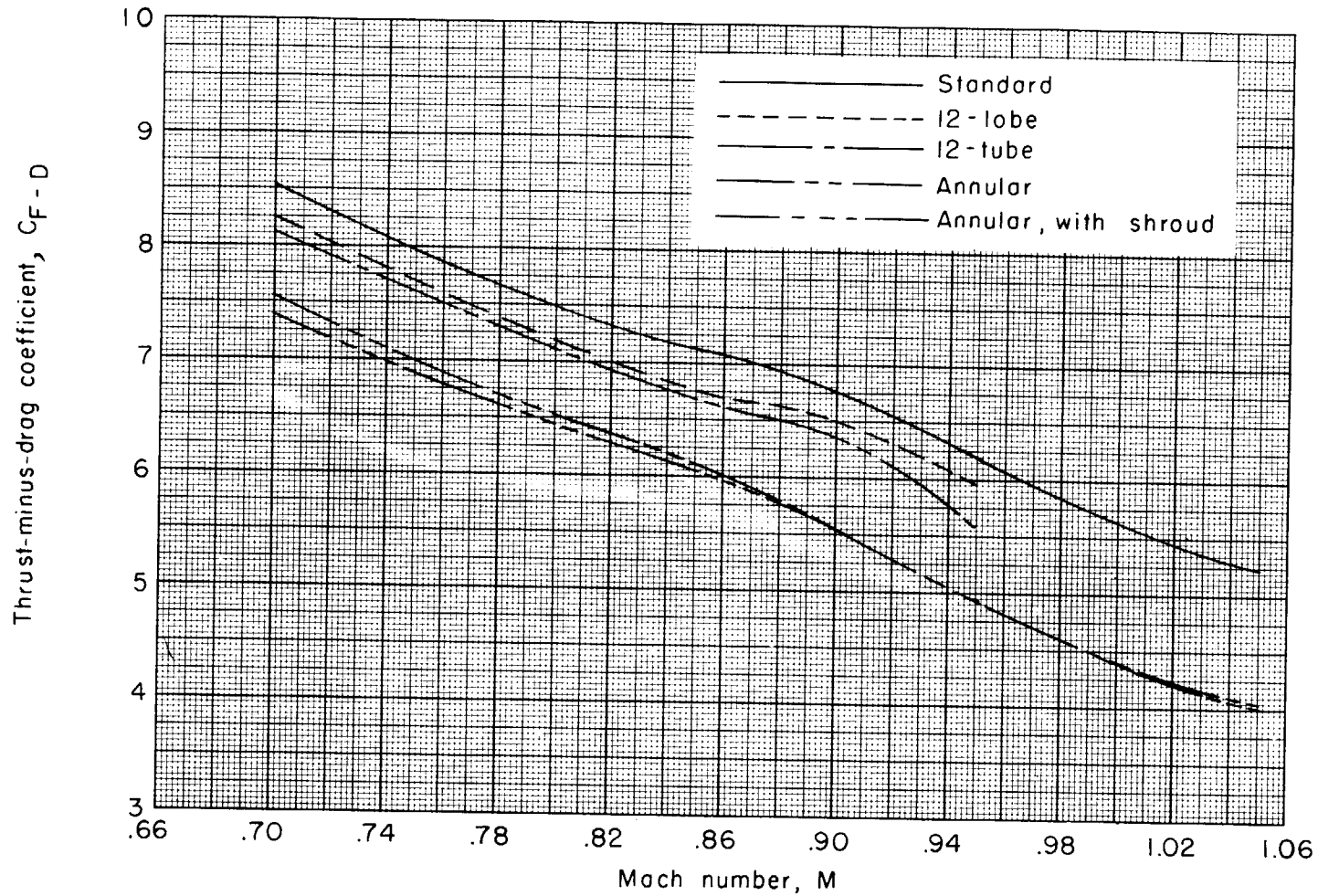

(a) Nonejector configurations.

Figure 11.- Variation of thrust-minus-drag coefficient with Mach number for assumed engine operating conditions.

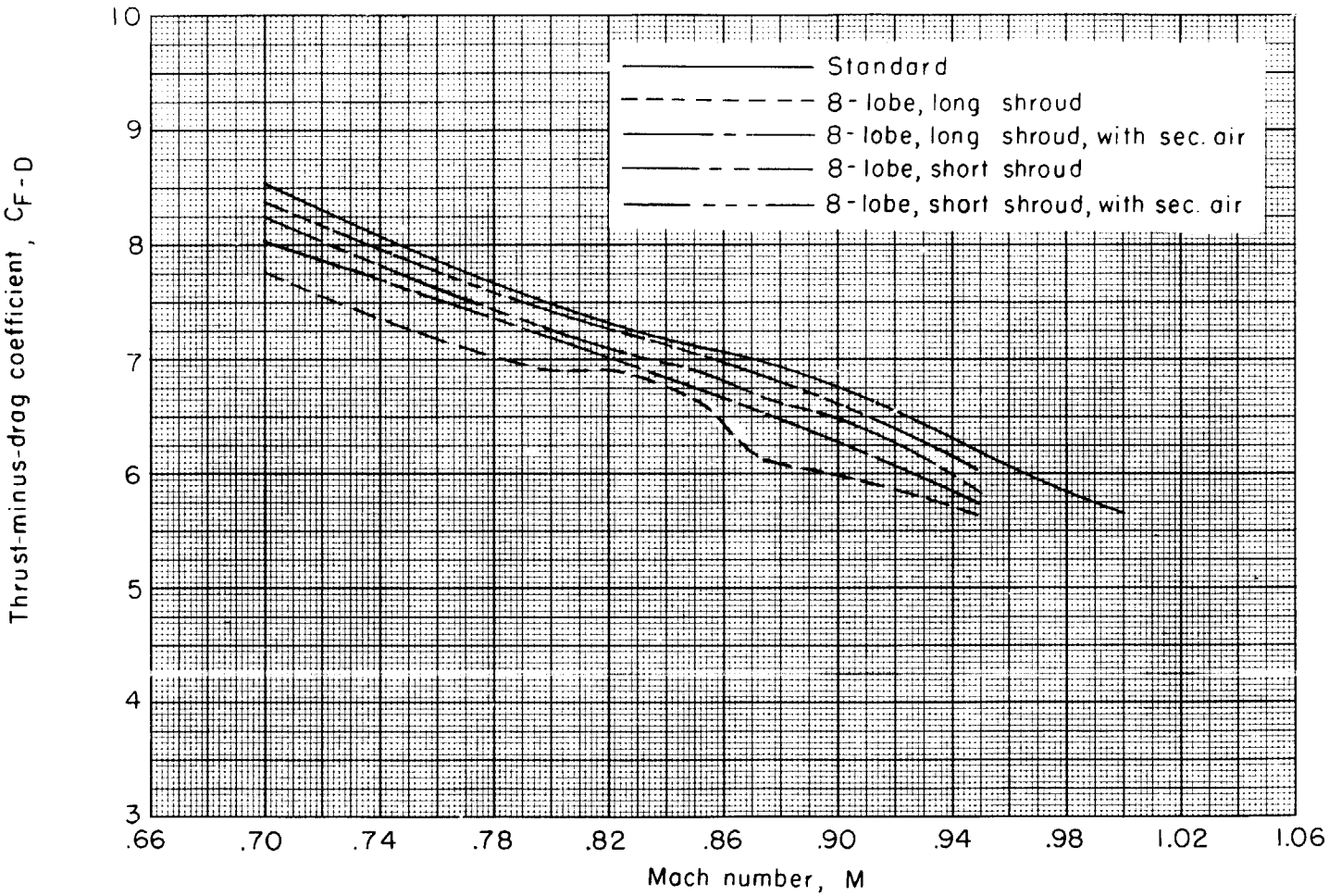

(b) Ejector configurations.

Figure 11.- Concluded.

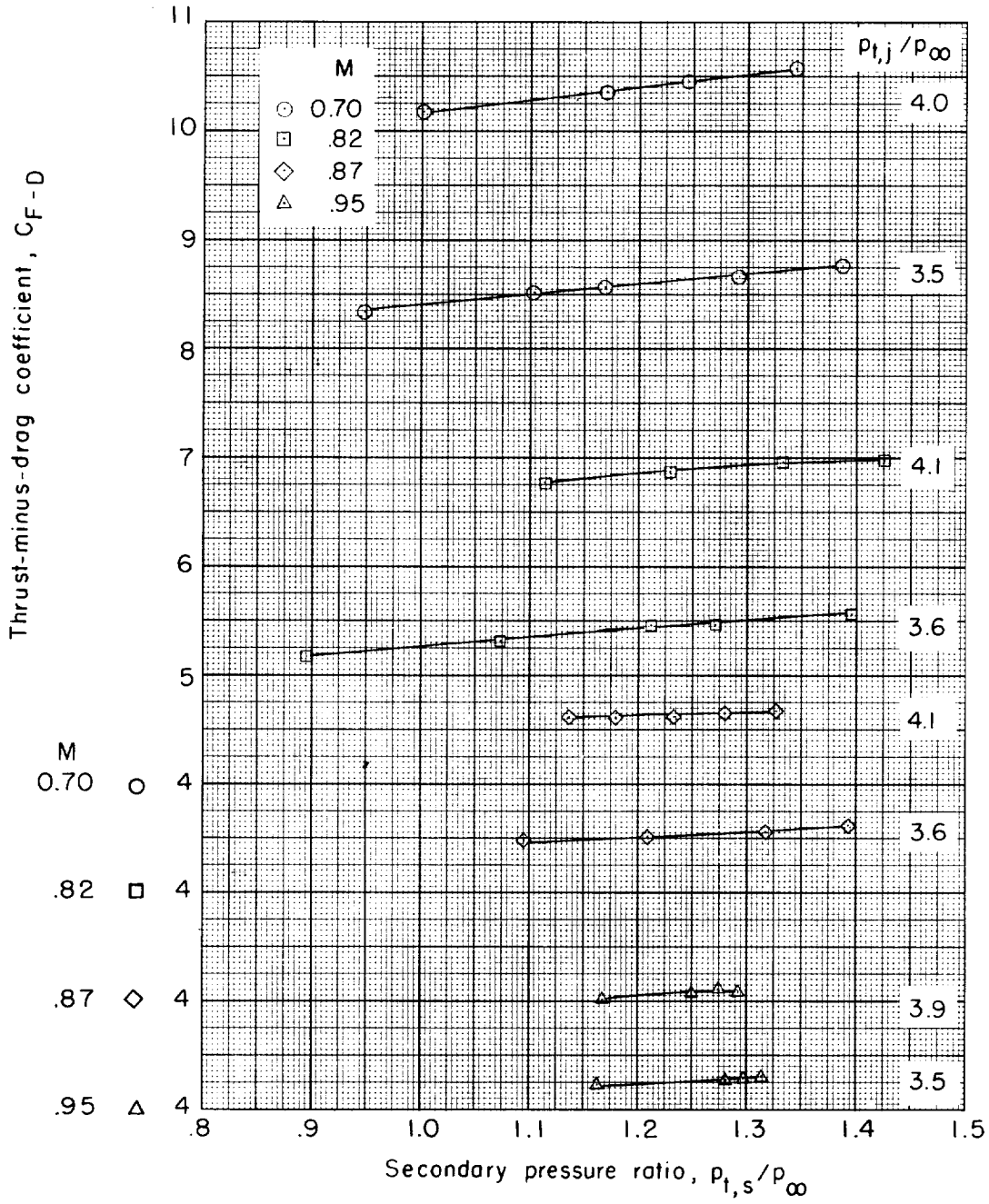

(a) Long shroud. $L/d_e = 0.284$.

Figure 12.- Variation of thrust-minus-drag coefficient with secondary pressure ratio for the 8-lobe noise-suppressor configuration.

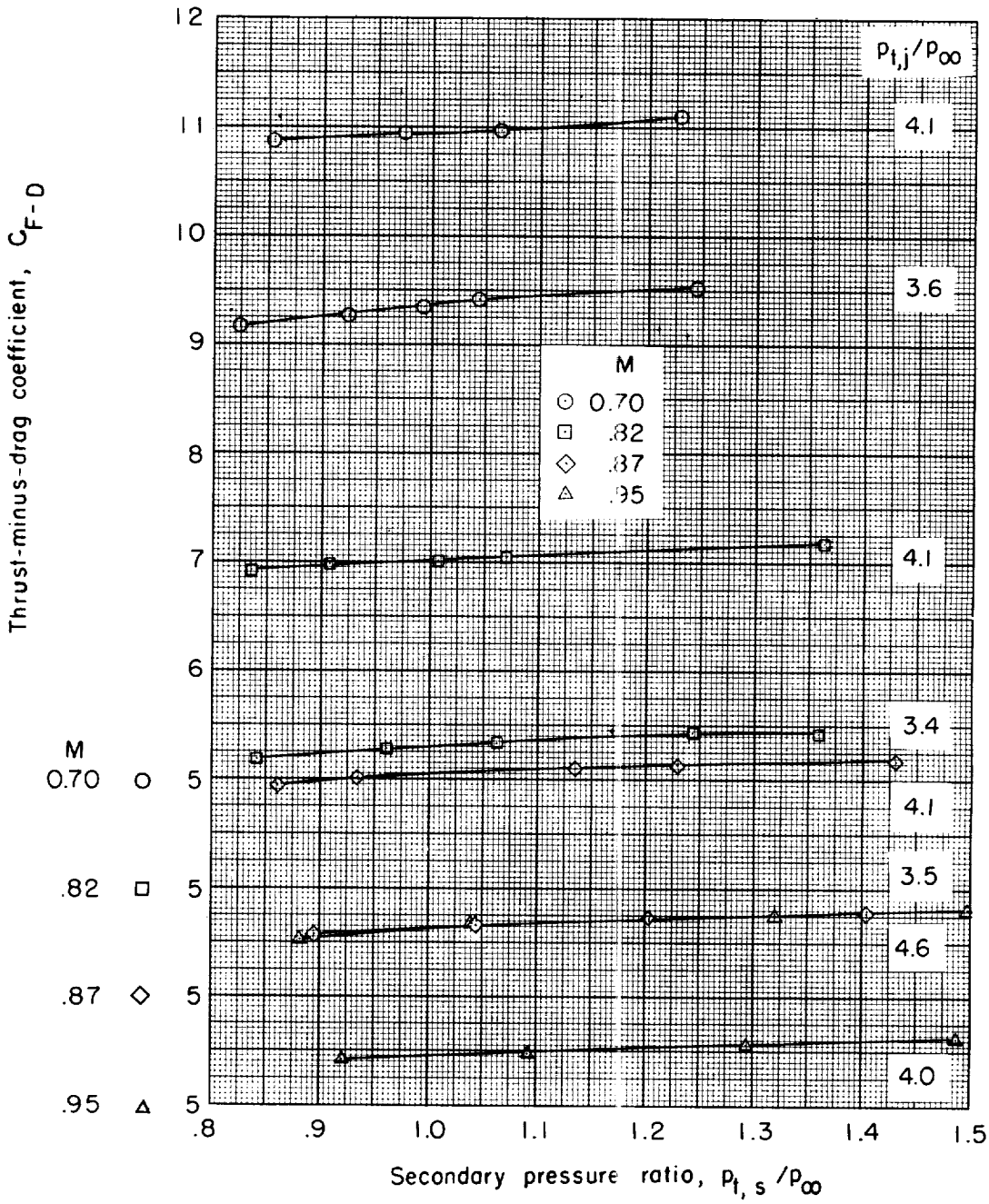

(b) Short shroud. $L/i_e = 0.044$.

Figure 12.- Concluded.

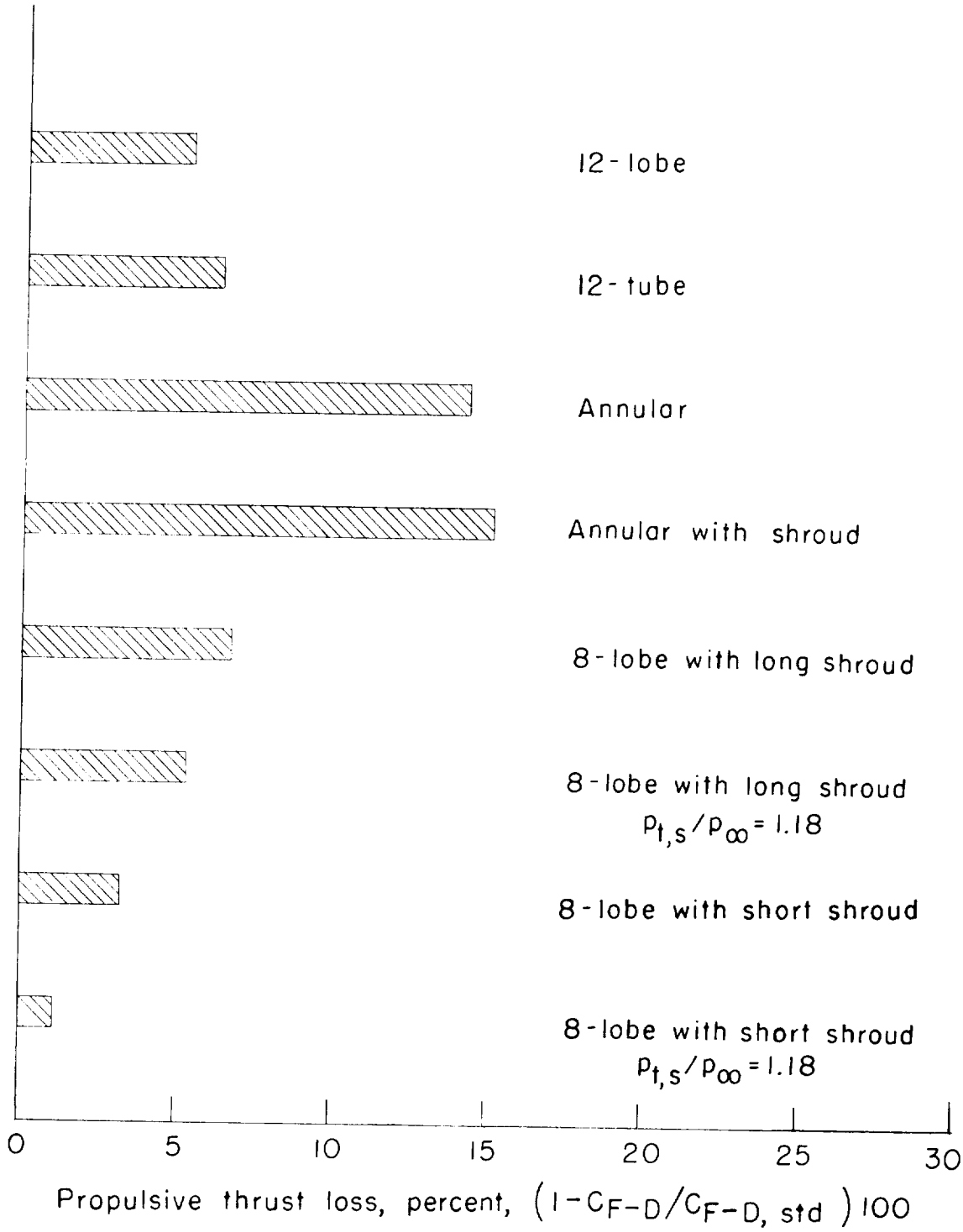

Figure 13.- Propulsive thrust comparison with standard nozzle as reference. $M = 0.85$; $p_{t,j}/p_\infty = 3.9$.

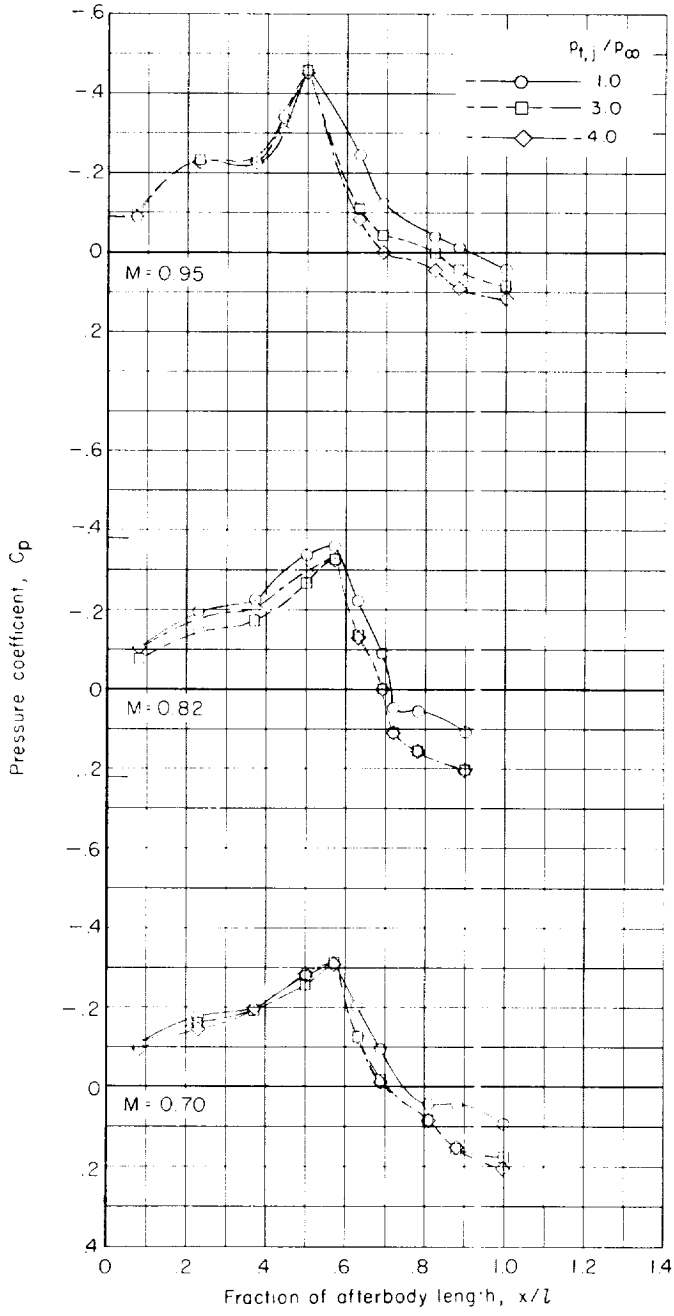

(a) Standard nozzle.

Figure 14.- Effect of pressure ratio on the pressure distribution of 90° row. Ticks indicate critical C_p.

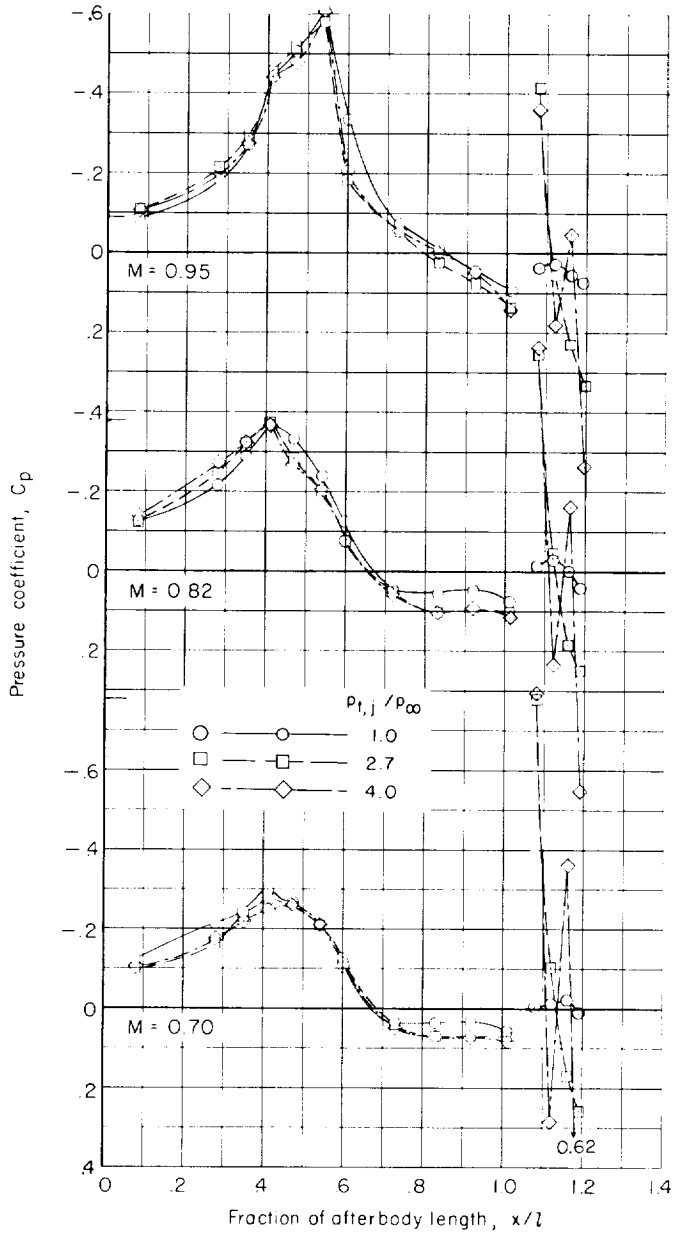

(b) Eight-lobe nozzle with long shroud. $L/d_e = 0.284$. No secondary flow.

Figure 14.- Concluded.

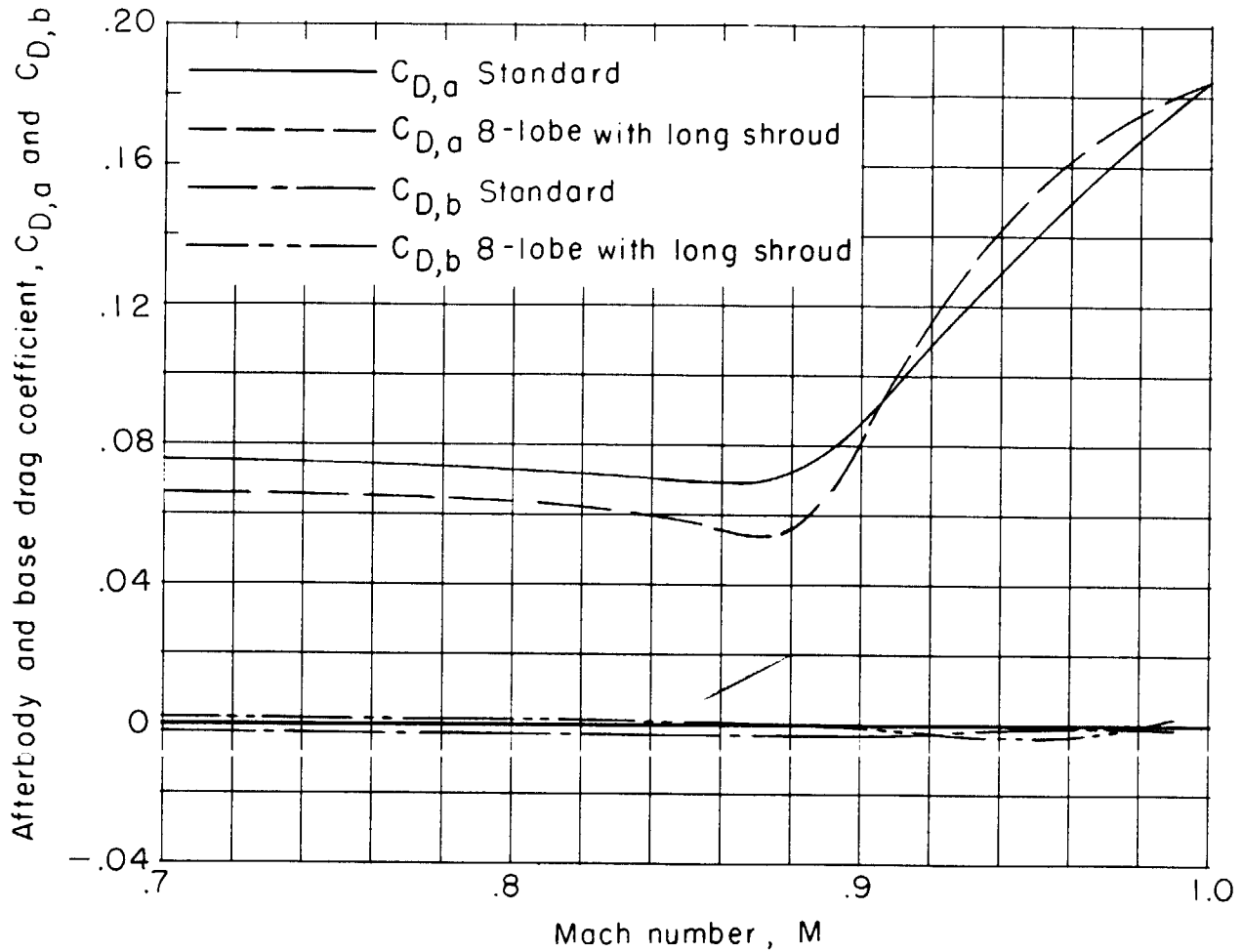

(a) $p_{t,j}/p_\infty = 1.0$.

Figure 15.- Variation of pressure drag coefficient with Mach number for standard and 8-lobe nozzles.

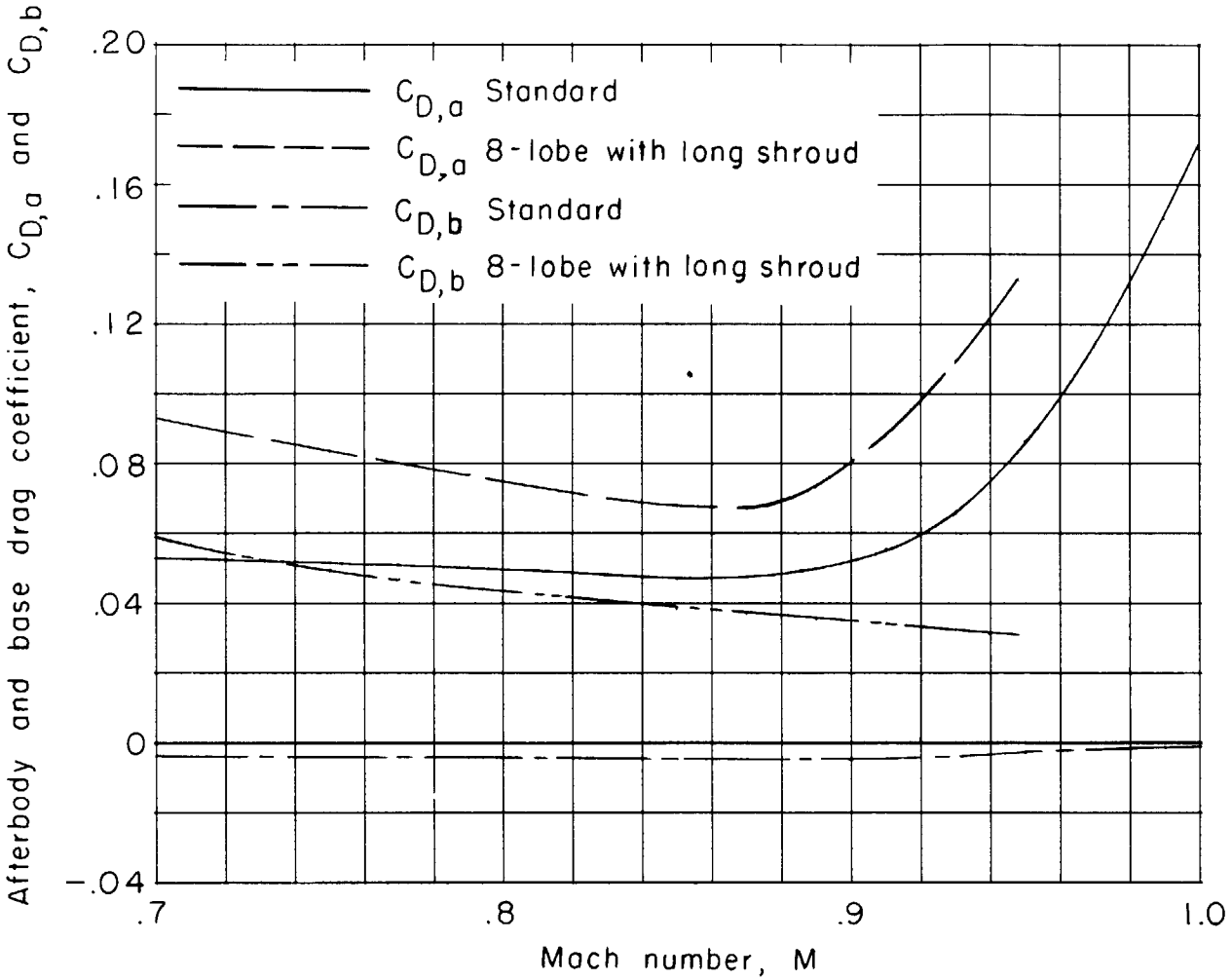

(b) $p_{t,j}/p_\infty = 3.0$.

Figure 15.- Continued.

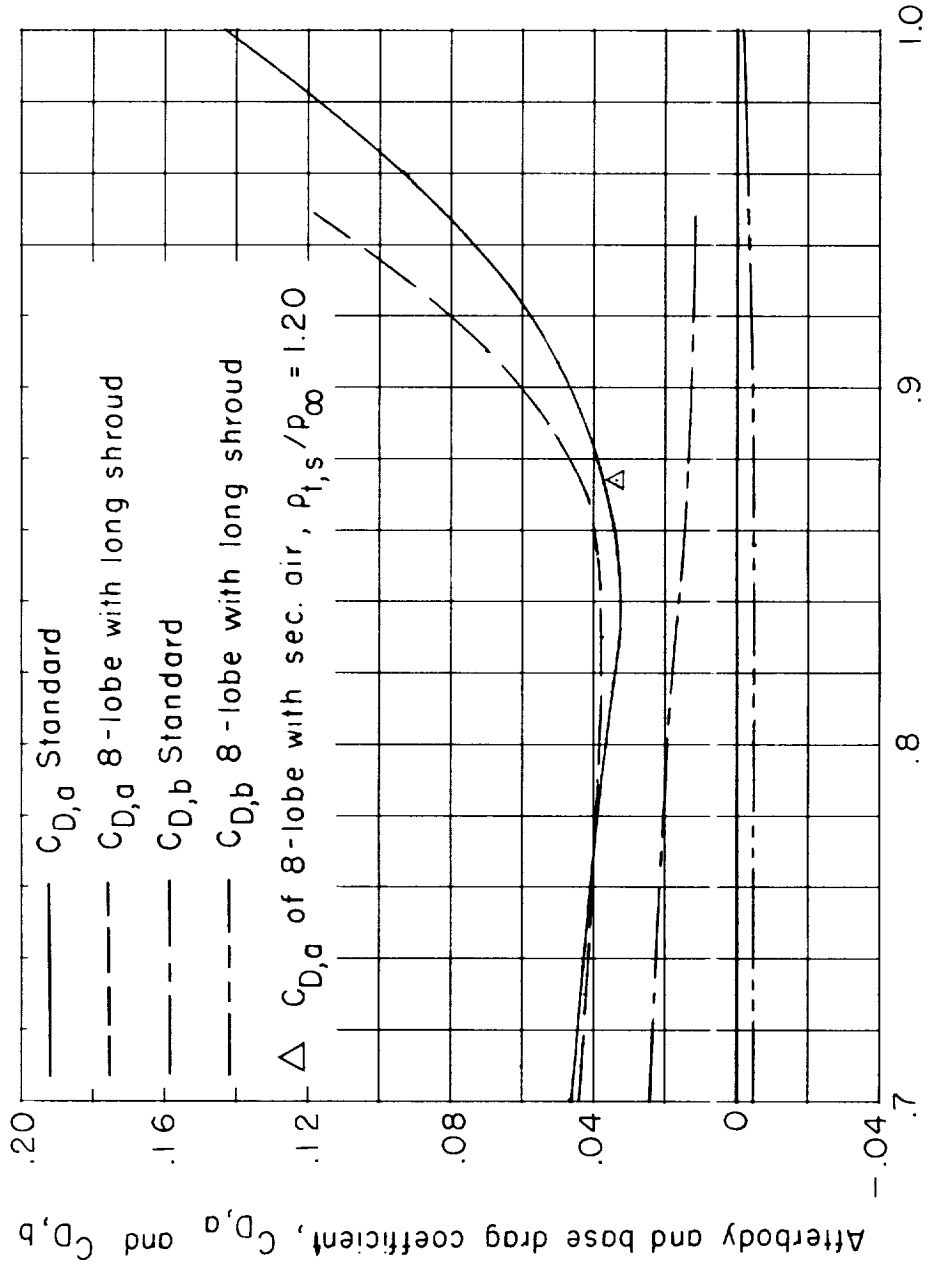

(c) $p_{t,j}/p_\infty = 4.0$.

Figure 15.- Concluded.